HHS Public Access

Author manuscript

Mol Cell. Author manuscript; available in PMC 2021 December 17.

Published in final edited form as:

Mol Cell. 2020 December 17; 80(6): 1025–1038.e5. doi:10.1016/j.molcel.2020.11.011.

The Smc5/6 core complex is a structure-specific DNA binding and compacting machine

Diego Serrano[1,*], **Gustavo Cordero**[#2], **Ryo Kawamura**[#3], **Aleksandr Sverzhinsky**[#4], **Muzaddid Sarker**[1], **Shamayita Roy**[1], **Catherine Malo**[1], **John M. Pascal**[4], **John F. Marko**[3], **Damien D'Amours**[1,5,†]

[1]Ottawa Institute of Systems Biology, Department of Cellular and Molecular Medicine, University of Ottawa, Roger Guindon Hall, 451 Smyth Rd, Ottawa, ON, K1H 8M5, Canada

[2]Département de pathologie & biologie cellulaire, Université de Montréal, C.P. 6128, succursale Centre-ville, Montréal, QC, H3C 3J7, Canada

[3]Department of Molecular Biosciences and Department of Physics & Astronomy, Northwestern University, Evanston, IL, 60208, USA

[4]Département de biochimie et médecine moléculaire, Université de Montréal, Montréal, Québec, H3C 3J7, Canada

[#] These authors contributed equally to this work.

Summary

The structural organization of chromosomes is a crucial feature that defines the functional state of genes and genomes. The extent of structural changes experienced by genomes of eukaryotic cells can be dramatic and spans several orders of magnitude. At the core of these changes lies a unique group of ATPases –the SMC proteins– that act as major effectors of chromosome behavior in cells. The Smc5/6 proteins play essential roles in the maintenance of genome stability, yet their mode of action is not fully understood. Here we show that the human Smc5/6 complex recognizes unusual DNA configurations and uses the energy of ATP hydrolysis to promote their compaction. Structural analyses reveal subunit interfaces responsible for the functionality of the Smc5/6 complex and how mutations in these regions may lead to chromosome breakage syndromes in

[†]Correspondence: damien.damours@uottawa.ca.

[*]Current address: Department of Pathology, Anatomy and Physiology, Faculty of Medicine – Solid Tumors Program, Center for Medical Applied Research; University of Navarra, Avenida Pio XII 55, 31008, Pamplona, Spain

[5]Lead Contact: Damien D'Amours

Author contributions

DS, RK, AS, JMP, JFM & DD conceived and designed the experiments; DS performed the *in vivo* fusion and XL-MS experiments; DS, MS & GC performed purifications, DNA-binding & enzymatic assays; GC carried out the analytical ultracentrifugation & GraFix procedures; AS & JMP performed EM imaging; RK carried out magnetic tweezers experiments; DS, SR & CM created yeast strains, assessed their viability & Smc6 abundance; DS, GC, RK, AS, JMP, JFM & DD analyzed the data; DS, RK, SR & AS prepared figures; DS & DD wrote the paper.

Declaration of Interests

The authors declare no competing interests.

humans. Collectively, our results suggest that the Smc5/6 complex promotes genome stability as a DNA micro-compaction machine.

Graphical Abstract

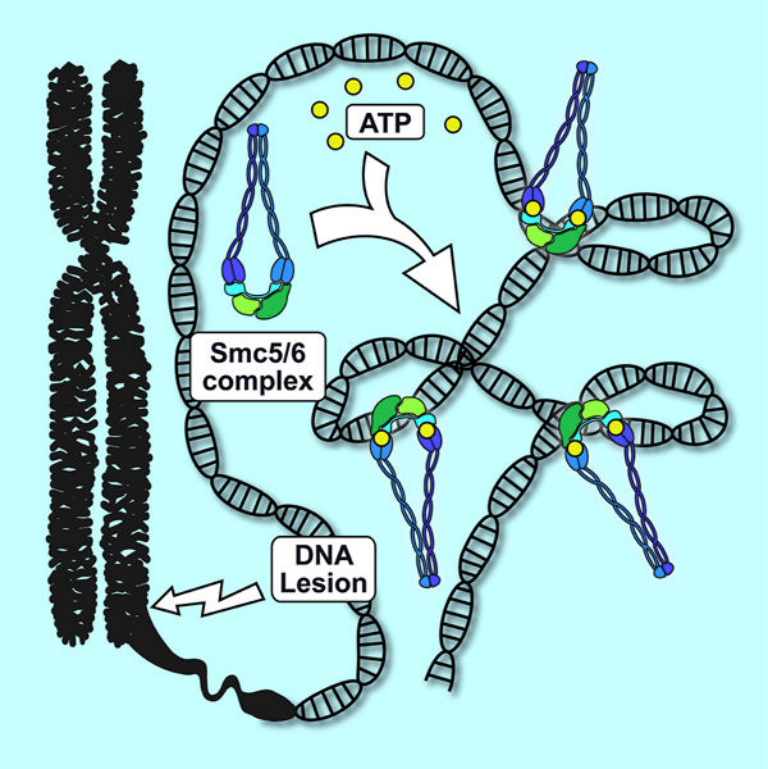

eTOC Blurb

The Smc5/6 complex is a crucial effector of chromosome integrity. Serrano *et al.* purified the human complex and show that it can recognize nucleic acids with unusual features. Smc5/6 can also use the energy of ATP hydrolysis to actively compact DNA substrates, thereby uncovering a mode-of-action for this important enzyme.

Introduction

Maintenance of genome integrity is an essential function for all living organisms. We know that several pathways act simultaneously *in vivo* to ensure the maintenance of genome integrity, but how these multiple pathways successfully integrate and/or coexist in time and space remains an outstanding question. Importantly, the ability to integrate disparate processes into an effective cellular response likely depends on the action of higher-order effectors that can modulate the physical conditions of the genome to allow multiple molecular transactions to operate simultaneously at a given genomic location.

The structural maintenance of chromosomes (SMC) family of proteins represents one class of higher-order effectors of genome organization that can coordinately regulate multiple processes *in vivo* (reviewed in Aragon, 2018; Baxter et al., 2019; Yatskevich et al., 2019).

These proteins are mechanochemical regulators of chromatin behavior and their activity is essential for the protection and dissemination of genomes in all species. SMC proteins assemble into large ring-like complexes that include cohesin (Smc1/3), condensin (Smc2/4) and the more recently discovered Smc5/6 complex. In eukaryotes, condensin participates in the compaction of chromosomes during cell division, whereas cohesin enforces proximity and alignment of sister chromatids (Yatskevich et al., 2019). The Smc5/6 complex, in contrast, plays diverse roles in the cellular response to DNA damage, but its exact contribution to genome stability is still unclear (reviewed in Aragon, 2018). A remarkable feature of the Smc5/6 complex is that, despite its crucial contribution to DNA repair, segregation and replication (Irmisch et al., 2009; Jeppsson et al., 2014; Potts et al., 2006), it is not a core factor essential for these individual processes under standard conditions. Instead, it appears to provide an integrative function that prevents toxic interactions involving distinct molecular pathways (Chen et al., 2009; Pebernard et al., 2006; Torres-Rosell et al., 2005).

How the Smc5/6 complex promotes chromosome integrity is a key unanswered question in the genome stability field. This gap in our knowledge can be explained in part by the difficulty in isolating pure Smc5/6 complex to perform in-depth mechanistic and structural studies. We report herein the development of an innovative co-translational folding strategy to purify the human Smc5/6 complex in its active form. Using this approach, we have discovered that the human Smc5/6 complex is a structure-specific DNA binding and compacting machine. An accompanying study (Gutierrez-Escribano et al., 2020) has found identical activities in the budding yeast complex, underscoring the conservation in the mode of action of eukaryotic Smc5/6 enzymes.

Results

A co-translational folding approach to assemble the human Smc5/6 complex

Previous studies from our laboratory and others have shown that the yeast Smc5-Smc6 dimer (Roy et al., 2015) as well as a number of human non-SMC elements of the complex (Nse1-Nse3; Doyle et al., 2010; Zabrady et al., 2016) can be purified as recombinant proteins. However, our initial efforts (as well as that of others; Zabrady et al., 2016) to purify soluble Nse4 monomer or recombinant Smc5/6 holoenzyme have been unsuccessful (Fig. S1A). This is likely due to the high number of hydrophobic clusters present in Nse4 (Fig. S1B), a central interaction hub within the Smc5/6 complex (Fig. 1A).

We considered the possibility that enforcing co-translational folding of hNse4a with other members of the Smc5/6 holoenzyme might facilitate complex assembly *in vivo* (Fig. 1A). To achieve this goal, we used a flexible linker to physically connect Nse4a with either Smc5 or Smc6, similar to a strategy previously employed to covalently close the cohesin ring (Gruber et al., 2006). Multiple TEV cleavage sites were introduced in the linker sequence between Nse4a and Smc5 or Smc6 to facilitate linker removal and recovery of individual subunits with native (or near-native) sequence after purification. We created two different yeast strains overexpressing Nse1 and Nse3 together with Nse4a-Linker-Smc5 or Smc6-Linker-Nse4a and their respective SMC partners (Fig. 1B). The hNse2 protein was not included in these complexes because it dissociates from the holoenzyme during mitosis (Behlke-Steinert

et al., 2009) and studies suggest that a non-negligible fraction of Smc5/6 complexes do not contain Nse2 (see gel filtration fractions 10 and 11 in Andrews et al., 2005). Consistent with this view, Nse2 is not essential for cellular viability in metazoans (*i.e.*, human, mouse and chicken cells; Kliszczak et al., 2012; Verver et al., 2016; Zheng et al., 2017), whereas all other components of the complex are (Aragon, 2018). The human complex containing Smc5/6 and Nse4/3/1 subunits corresponds to the canonical organization of other SMC complexes (condensin and cohesin; reviewed in Yatskevich et al., 2019), and we will hereafter refer to this form of the enzyme as the Smc5/6 core complex. As a control, we constructed an additional overexpression strain specific for the SMC scaffold of the enzyme, the Smc5/6 dimer.

Purification of functional Smc5/6 dimer and core complex

We took advantage of a yeast co-overexpression system developed in our laboratory (Roy et al., 2011; St-Pierre et al., 2009) to isolate the Smc5/6 heterodimer to near homogeneity (Fig. 1C). Importantly, the stoichiometry of the SMC subunits was 1:1 after our purification, reflecting the stability of subunits and proper dimerization through the hinge domain. Small purification tags were not removed from Smc5 and Smc6 since previous work from our laboratory showed that the Smc5/6 dimer is not adversely affected by fusion with multi-histidine and Strep-tagII sequences (Roy and D'Amours, 2011; Roy et al., 2011).

We next proceeded to purify the Smc5/6 core complex using the fusion approach described above. We focused our initial efforts on complexes containing the Nse4-Linker-Smc5 fusion protein (Fig. 1B). We were able to purify soluble recombinant Smc5/6 core complex using a combination of nickel-chelate (Ni-NTA), StrepTactin and glutathione affinity chromatography steps (Figs. 1D, S2A). After cleaving the purification tags (on Nse1, Nse4a and Smc6) and linker sequence connecting Nse4 and Smc5, we performed size exclusion chromatography on Superose 6 as a final step to remove TEV protease and tag remnants (Figs. 1D, S2B). This co-translational expression/folding strategy enabled the purification of soluble Smc5/6 core complex to high levels and near homogeneity (≥95%). Rate-zonal centrifugation of the purified Smc5/6 core complex revealed its subunits sedimented in fractions corresponding to a mass of 300–400 kDa, a range that is consistent with a monomeric complex (*i.e.*, predicted mass = 365 kDa; Figs. 1E, S3A,B).

The Nse4-Smc5 fusion is functional in vivo

We next wanted to determine whether fusion of Nse4 with SMC subunits is compatible with assembly and full functionality of the Smc5/6 complex *in vivo*. To test this possibility, we expressed Nse4-Linker-Smc5 and Smc6-Linker-Nse4 fusion proteins in the budding yeast *Saccharomyces cerevisiae*. Sporulation of heterozygous diploid strains carrying *NSE4/nse4Δ SMC5/smc5Δ* showed that expression of the yeast *NSE4-Linker-SMC5* fusion protein can complement cell lethality in spores carrying both *smc5Δ* and *nse4Δ* (Fig. 2A). Moreover, *smc5Δ nse4Δ* mutants expressing the yeast Nse4-Linker-Smc5 protein showed wild-type kinetics of cell proliferation in the presence or absence of DNA damaging agents (Fig. 2B–C). Since the Smc5/6 complex is required for cell viability and DNA repair, we infer from these results that fusing Nse4 to Smc5 does not adversely affect the functionality of the complex.

Arm configuration of the Smc5/6 complex

We took advantage of our purified complex to visualize the general morphology and arrangement of Smc5/6 subunits by negative stain transmission electron microscopy (EM). To ensure the structural integrity of Smc5/6 complexes used in our EM experiments, we first fractionated the enzyme by sucrose density centrifugation and subsequently imaged a single fraction corresponding to monodisperse core complexes (*i.e.*, fraction 7; Figs. 1E, 3A). Image analysis revealed that particles corresponding to the entire Smc5/6 complex adopted a rod conformation rather than a ring shape (Fig. 3B,E). Since the majority of observed particles were smaller than expected, we decided to use mild chemical crosslinking (GraFix) to rule out the possibility that the conformation observed for the Smc5/6 complex was due to an artifact of grid preparation and/or complex dissociation. The GraFix procedure stabilizes the structure of protein complexes by virtue of progressive fixation in a sucrose gradient containing a low concentration of glutaraldehyde (Fig. S3C)(Kastner et al., 2008; Stark, 2010). Upon completion of GraFix ultracentrifugation, fractions corresponding to the pentamer (*i.e.*, fraction 7; compare Figs. 1E/S3A and 3A/S3C) migrated as a single high-molecular mass band on SDS-PAGE gels, indicating efficient intra-complex crosslinking without inter-complex aggregation (Fig. 3A).

We then proceeded to EM image acquisition after negative staining of the stabilized complex. As expected, the GraFix samples showed an increased numbers of SMC-like particles per micrograph. Importantly, image analysis confirmed that the Smc5/6 core complex adopted a closed arm configuration with two globular domains (corresponding to the hinge domain, on top; and the Nse1/3/4 subcomplex, bottom) linked by a rod structure (corresponding to the coiled-coil [CC] arms of Smc5/6; Fig. 3C,F). This morphology is visually analogous to that of two cherries connected to a single stem. Dimensions of the complex are slightly smaller than those of condensin and cohesin (namely ~450 x 140 Å), consistent with the shorter CC arms of Smc5 and Smc6 proteins (as predicted by Burmann et al., 2017; Fig. 3B–C,E–F). The resultant three-dimensional EM map of the Smc5/6 complex revealed that the size and shape of the globular regions on each end of the rod-shaped complex dovetail nicely with the dimensions of the Nse1/3 dimer and yeast Smc5/6 hinge domain observed in crystal structures (Fig. S4A–F; Alt et al., 2017; Doyle et al., 2010). These observations suggest that the morphology reported here reflects a native configuration of the Smc5/6 complex.

The Smc5/6 dimer also appeared as a rod shaped-particle by negative stain EM, but we noticed that the SMC arms demonstrated more flexibility in the dimer than in the core complex (Fig. 3D,G). In some cases, it was possible to distinguish individual CC arms or kinks in the arms of the dimer in single particle images. This apparent increase in the flexibility of SMC arms is consistent with the absence of kleisin subunit in the Smc5/6 dimer, a condition that is expected to relieve structural constraints normally present on SMC arm movement. Taken together, these experiments reveal that subunits of the Smc5/6 core complex assemble into a rod-like structure that favors a colinear/closed arm configuration for the SMC subunits.

Mapping contact points among the subunits of the Smc5/6 complex

We used small chemical probes to explore the landscape of contact points among the subunits of the Smc5/6 complex. The purified dimer and core complex were exposed to agents that crosslink (XL) lysines to other residues and reactions were subsequently processed by mass spectrometry (MS), as performed previously (Courcelles et al., 2017). In this analysis, XLs are formed between different amino-acid residues based on their proximity within the Smc5/6 complex, thereby indicating connection points or transient interfaces among subunits.

Graphical maps displaying the network of subunit connections identified by XL-MS are shown in Figure 3H–I, whereas the complete list of 158 intra- and inter-subunit connections identified in our experiments is included in Table S1. Analysis of the landscape of connections in these maps confirmed that the dimer is highly flexible in solution, which is demonstrated in proximity maps as a low frequency of interaction for residues of different SMC subunits (Table S1, 9 XLs; Fig. 3I, colored lines). In comparison, when the movement of SMC arms is constrained by the kleisin subunit in the core complex, connections involving different SMC proteins were more than twice as abundant (Table S1, 20 XLs; Fig. 3H). These observations are consistent with the level of SMC arm flexibility that we noticed in EM experiments (Fig. 3B–G).

A large fraction (~60%) of the long-range connections that we identified are consistent with the known structure of SMC complexes, thereby validating the quality of the XL-MS results. For example, the XL-MS analysis revealed several connections involving the hinge domains of the two SMC subunits (*e.g.*, Smc5-K542 with Smc6-K628; Fig. 3H, orange lines). We also detected several predicted intra-molecular connections among the α-helical regions that form the CC arms of individual SMCs (Fig. S4G,H). Our EM data showed that the SMC arms of Smc5 and Smc6 were in close proximity to each other in the holoenzyme, an observation independently confirmed by our XL-MS data (see inter-subunit XL connecting Smc5/6 CC arms; Smc5-K232/K247/K300/K783 with Smc6-K234/248/K310/K821, respectively; Figs. 3H, S4I).

Beyond the XLs connecting SMC proteins together, our analysis revealed a rich network of connections linking functional domains of NSE subunits with other parts of the complex, such as the winged-helix (WH) domains of Nse3 and the N-terminal ATPase domain/CC neck of Smc6 (Fig. 3H). The α helical region of Smc6 acted as a connection hub for all but one subunit of the core complex (*i.e.*, Nse1), suggesting an important role in the regulation of complex activity or topology. We also detected several contact points involving Nse3 to Nse1, as predicted from the structure of the dimer (Doyle et al., 2010). Our XL-MS data suggest that Nse4 in combination with Nse1 and Nse3 is capable of bridging the ATPase/CC neck regions of Smc5 and Smc6.

Functional relevance of contact points in Smc6 and Nse3–4 subunits

Next, we investigated the physiological significance of contact points that we identified in the WH domain of Nse3 and other parts of the complex. This region is of particular interest because it contains mutations responsible for the lung disease, immunodeficiency, and

chromosome breakage (LIC) syndrome (Fig. 4A–C; van der Crabben et al., 2016). Based on the evolutionary conservation of the crosslinked positions and nearby residues, we inserted several mutations in the *NSE3* locus in *S. cerevisiae* (Fig. 4B,C) and assessed the ability of the resulting mutant strains to proliferate in the presence of DNA damaging agents (Fig. 4D).

Yeast strains carrying mutations in the WH-B extension domain of Nse3 demonstrated a strong conditional defect in their ability to grow on media containing genotoxic agents like MMS, HU or 4NQO (Fig. 4D). Whereas the proliferation of *nse3-E265R* and *nse3-L268K* mutant appeared normal on media containing DNA damaging agents at 23 °C, the growth capacity of these strains became severely affected at 37 °C (Fig. 4D). In fact, yeast strains carrying the *nse3-E265R* allele were sensitive to all DNA damaging agents tested, whereas the growth of *nse3-L268K* mutants was strongly impaired in the presence of MMS at 37 °C. Importantly, the *nse3-E265R* and *nse3-L268K* mutations map to a highly conserved α helix in the WH-B extension domain and are located very close (*i.e.*, less than 12 Å and 6 Å, respectively) to a residue mutated in LIC syndrome patients (Fig. 4C, inset). From a functional perspective, the corresponding hNse3 residues represent contact points with the N-terminal ATPase domain of Smc6 in our XL-MS data (Fig. 3H). We also noticed that the same region of Smc6 (together with the adjacent CC neck) shared reciprocal connections with other residues in the WH domain of hNse3. This suggests the existence of an interaction hub for Nse3 in the ATPase/CC neck of Smc6.

To test the idea proposed above, we introduced mutations in residues of yeast Smc6 that correspond to those interacting with the WH domain of Nse3 (*i.e.*, positions marked in Fig. S4G). As predicted, yeast expressing the *smc6-R135E* and *smc6-R144E* alleles showed severe sensitivity to DNA damaging agents at 37 °C (Fig. 4D). We also constructed a yeast strain carrying a D261A mutation in Nse4, another putative Smc6-proximal residue. The *nse4-D261A* mutants showed growth defects highly reminiscent of those seen in *smc6* and *nse3* mutants (Fig. 4D), underscoring their common hypomorphic defect. Remarkably, mutation in arginine 144 of Smc6 led to a substantial decrease in protein abundance at non-permissive temperature (Fig. 4E–F), a phenotype similar to the protein stability defect observed in subunits of the Smc5/6 complex of LIC syndrome patients (van der Crabben et al., 2016). Together, these results indicate that residues at the interface of Nse3–4 and the ATPase/CC neck region of Smc6 are important for the activity of the Smc5/6 complex.

Structure-specific DNA recognition and binding by the Smc5/6 complex

Previous findings from our laboratory revealed that yeast Smc5 and Smc6, as well as the Smc5/6 dimer, have intrinsic DNA-binding activity (Roy and D'Amours, 2011; Roy et al., 2015; Roy et al., 2011). However, the substrate preference and affinity of the human Smc5/6 dimer and core complex remain to be established.

We focused our initial analysis on the Smc5/6 dimer to define the baseline DNA binding activity of these SMC proteins. We specifically monitored the affinity of Smc5/6 for double-stranded (ds) and single-stranded (ss) DNA substrates using electrophoretic mobility shift assays (EMSAs), as previously described (Roy et al., 2015). The nucleotide content of ss and dsDNA substrates used in this assay is roughly similar, thus allowing a direct

comparison of Smc5/6 affinities for these substrates. Figure 5A shows that the Smc5/6 dimer exhibited different DNA binding behavior when ss and ds substrates were used. The affinity of the dimer was markedly higher for ssDNA substrates than for duplex DNA. For example, Smc5/6 could fully bind the ssDNA substrate at 48-fold molar excess, whereas equivalent saturation was only attained at 400-fold excess of dimer relative to the nucleotide content of the dsDNA (Fig. 5A).

Next, we asked if non-SMC elements (Nse4a/3/1) contribute to the DNA-binding properties of the Smc5/6 core complex. It has been shown previously that the human Nse1/Nse3 dimer can bind various types of DNA (Zabrady et al., 2016), but whether this role can be performed by these subunits in the context of the Smc5/6 complex is still unknown. Our results indicate that the presence of the regulatory subunits does not alter the basal DNA-binding activity of the Smc5/6 dimer. As shown in Figure 5A–B, the affinity of the core complex for ssDNA is similar to the K_d of the dimer (32.4 nM ± 1.9 nM dimer, 27.3 nM ± 0.76 nM core complex; Fig. S5A). From a qualitative standpoint, however, the nature of the binding by the core complex appeared different than that of the SMC dimer. The presence of the NSE elements in the core complex allowed the formation of intermediate DNA-protein species in the gel (*i.e.*, partially-retarded DNA; line with asterisk) which were not formed when the SMC dimer associated with ssDNA (Fig. 5A *vs* 5B; left) or were formed at a much lower abundance when the SMC dimer associated with dsDNA substrates (Fig. 5A *vs* 5B; center). Moreover, compared to the SMC dimer alone, NSE proteins lowered the dissociation constant of the core complex for dsDNA (121 nM ± 7 nM dimer *vs* 81.8 nM ± 3.04 nM core complex; Fig. S5A).

We next sought to test whether the Smc5/6 complex is capable of binding small 60 bp DNA duplexes in EMSA experiments. We included RNA/DNA hybrids in this analysis since Smc5/6 was proposed to interact with this type of nucleic acid in the early stages of DNA replication (Lafuente-Barquero et al., 2017). We found that the Smc5/6 complex is able to bind both hybrid and dsDNA with similar affinity (Fig. 5C). RNA/DNA hybrids appeared to be slightly better binding partners for the Smc5/6 core complex than DNA duplexes, but this trend was not statistically significant. Together, our DNA-binding experiments indicate that the Smc5/6 complex can associate with non-B form DNA conformations with high affinity.

The Smc5/6 core complex compacts DNA against force in an ATP-dependent manner

Next, we wanted to determine if the Smc5/6 complex was capable of remodeling the configuration of DNA in space. In order to monitor DNA compaction by the Smc5/6 core complex, we carried out single-DNA magnetic tweezers experiments (Keenholtz et al., 2017). This approach uses 10 kb end-labeled DNA molecules tethered to a cover glass at one end, and to a paramagnetic bead at the other end. Molecules were tethered inside flow cells, allowing solvent conditions in the vicinity of the DNA to be changed, and a nearby magnet was moved to vary the pulling force applied to the paramagnetic particle (Fig. 6A). A typical experiment started with DNA under 2 pN tension (a high enough force to pull nearly all bending fluctuations out of the DNA) in Smc5/6-free buffer. Then Smc5/6 core complex plus cofactors were introduced into the flow chamber, force was reduced to that under study, and the kinetics of the change in DNA extension were observed.

In the absence of Smc5/6 complex, DNA extension was stable for DNA tensions from 2 pN down to 0.3 pN. When 5 nM Smc5/6 core complex was added to the buffer in the absence of nucleotide, the DNA extension was stable and unchanged from its initial protein-free value as force was reduced (Fig. 6B; 5 nM Smc5/6 complex, 0 mM ATP). When the same experiment was performed with 1 mM ATP, DNA compaction was observed at a rate markedly dependent on force (Fig. 6C, 5 nM Smc5/6 complex, 1 mM ATP). Note that the compaction at 0.3 and 0.5 pN proceeds at a high rate and that the initial stages of the dynamics are in fact difficult to see in Figure 6C. At higher forces, individual steps are clearly visible (Fig. 6C, cyan 1 pN curve). Quantification of step size from a series of four 1 pN experiments led to an estimated step size of 90±10 nm, similar to that observed for condensin and cohesin complexes (Eeftens et al., 2017; Keenholtz et al., 2017; Strick et al., 2004; Sun et al., 2013).

We next examined ATP-dependent compaction rates of the Smc5/6 core complex as a function of force (Fig. 6D). A strong suppression of compaction rate was observed when force increased above 0.5 pN, which is characteristic of a compaction reaction that depends on the capture of DNA loops (Keenholtz et al., 2017; Marko et al., 2019; Skoko et al., 2006; Sun et al., 2013). The total amount of compaction of the DNA (the ratio of the total change in extension during the compaction reaction to the initial extension) also showed a strong force dependence, again suppressed by forces ≥ 1 pN (Fig. 6E).

Given that the 0.5 pN reactions were in the midrange of compaction rate and total DNA compaction, we measured the amount of compaction at 0.5 pN for different nucleotide cofactors, relative to the case of 1 mM ATP (Fig. 6F, leftmost bar). When ATP was entirely omitted (2nd bar), DNA compaction was almost completely suppressed; the same effect was seen in the presence of 1 mM ADP (3rd bar) or when non-hydrolysable ATPγS was included in the reaction. These experiments are consistent with the fact that purified Smc5/6 enzyme is active as an ATPase in solution (below). We thus conclude that compaction of DNA against sub-piconewton forces by the Smc5/6 core complex requires nucleotide as well as nucleotide hydrolysis, and that the critical force that suppresses that compaction is approximately 1 pN.

Supercoiled DNA is a high affinity substrate for the Smc5/6 core complex

The observations that yeast and human Smc5/6 dimers can recognize structured DNA (Fig. 5; Roy and D'Amours, 2011; Roy et al., 2015; Roy et al., 2011) prompted us to investigate whether purified Smc5/6 core complex can preferentially bind to supercoiled DNA. We designed a "plectonemic supercoil capture" experiment (Fig. 7A), using the principle that when DNA is twisted while held under relatively low force (~0.3 pN), it will buckle when sufficiently twisted, and then form plectonemic supercoils, with each successive turn past the buckling point reducing the overall extension of the DNA molecule by about 50 nm (Strick et al., 1996). For the naked 10 kb DNAs used in this study, a linking number change (ΔLk) of +30 or −30 will induce a reduction in DNA extension of approximately 1200 nm; when ΔLk is returned to 0, this reduction in extension ceases because the DNA returns to its initial untwisted configuration.

To visualize the effect of the Smc5/6 complex on plectoneme dynamics, we used modified reaction conditions that do not allow the complex to compact DNA when ΔLk is set at 0 and low forces are applied on DNA (*i.e.*, no torsional stress; left purple points in Fig. 7B). Under these conditions, protein-DNA interactions are likely weakened to the point that the Smc5/6 complex was unable to capture loops of DNA (see Fig. S5B for details). However, when we changed DNA linking number to ΔLk = −30 (Fig. 7B, blue points), waited for 30 seconds (Fig. 7B, green points), then returned to ΔLk = 0 (Fig. 7B, right purple points), DNA extension returned to a value about 1000 nm smaller than the starting point, consistent with supercoils being "captured" by the Smc5/6 core complex. We observed similar behavior for positive supercoiling (Fig. 7C). In the absence of ATP, we could repeatedly cycle ΔLk between 0, +30, 0 and −30 without observing any "capture" events (Fig. 7D).

To characterize in detail the DNA supercoil-binding behavior of the Smc5/6 core complex, we carried out a series of single-molecule capture experiments where we specifically monitored the length of plectonemic DNA "stabilized" via supercoil binding/capture (Fig. 7A). The left group of bars in Figure 7E shows the reduction of length experienced by naked DNA after ΔLk of +30 and −30 (*i.e.*, step 2 in Fig. 7A). This reduction in length corresponds to the plectoneme size and is similar for the two directions of rotation; approximately 1200 nm. The central group of bars shows the reduction in length in the presence of 5 nM Smc5/6 core complex for ΔLk of +30 or −30 (*i.e.*, step 3 in Fig. 7A); again all the reductions in length are approximately 1200 nm indicating that the Smc5/6 core complex did little to perturb the extended length of plectonemic DNA formed under these conditions. However, the right group of bars shows that when ΔLk was returned to 0 (*i.e.*, step 4 in Fig. 7A), supercoils "captured" by Smc5/6 core complexes stabilized DNA in a plectonemic configuration (Fig. 7E). This "capture" effect was completely dependent on the presence of ATP in the reaction buffer, since DNA extension returned to its maximal/unfolded value – which reflects a plectoneme size of zero– in the absence of nucleotide. The amount of capture was on average equal for ΔLk of +30 or −30, with no apparent strong preference for one handedness or the other (Fig. 7E). The Smc5/6 core complex was capable of maintaining the captured DNA in a plectonemic configuration against forces up to 2 pN (Fig. S5C). We conclude that under conditions where DNA is not compacted, the Smc5/6 core complex can efficiently bind and "capture" DNA supercoils in the presence of ATP, consistent with *in vivo* observations (Kegel et al., 2011). The effect of ATP in plectoneme stabilization experiments does not strictly imply a hydrolysis effect as it could also reflect ATP-mediated modulation of Smc5/6 complex binding to DNA.

Discussion

Compared to other SMC complexes, the Smc5/6 complex has remained an enigmatic effector of chromosome stability since its discovery. Whereas the core biological functions of cohesin and condensin are well defined, the involvement of the Smc5/6 complex in multiple, apparently distinct cellular processes has not allowed the emergence of a unified model to explain its unique contribution to genome stability (reviewed in Aragon, 2018).

Here we report for the first time how the human Smc5/6 complex recognizes and then modulates DNA structure in space. Our biophysical analyses suggest that the multi-

functional nature of the Smc5/6 complex is achieved *in vivo* by compacting chromosomal regions containing unusual DNA structures. This compaction is focussed on specific DNA structures (*i.e.*, local in nature), and we will thus refer to this process as "micro-compaction" to differentiate it from the global compaction seen in mitosis. We envision that the micro-compaction activity of the Smc5/6 complex will have at least two effects *in vivo*; first, it will create a physical barrier –steric hindrance– that will shield DNA intermediates from the action of undesirable modifying enzymes, and second, it will promote physical proximity of DNA molecules as a means to enhance biochemical reactions. The combined result of these two processes will be the stabilization and rapid repair of DNA intermediates that would otherwise have a propensity to degenerate into toxic DNA lesions when unprotected (Chen et al., 2009; Pebernard et al., 2006; Torres-Rosell et al., 2005). The repair of RNA-DNA hybrids –or R-loops– represents a salient example of a process that could benefit from the DNA compaction activity of the Smc5/6 complex. Indeed, R-loop repair requires the reannealing of separated ssDNA molecules (Garcia-Muse and Aguilera, 2019) and DNA compaction by the Smc5/6 complex might enhance formation of dsDNA by bringing complementary ssDNA together in a smaller effective volume, thus increasing the likelihood of their interaction. This prediction is consistent with our demonstration that the Smc5/6 complex can bind to RNA-DNA hybrids and ssDNA molecules, as well as genetic evidence connecting the complex to R-loop repair *in vivo* (Styles et al., 2016). We envision that the contribution of Smc5/6-mediated micro-compaction in DNA transactions will not be limited to R-loop repair and will likely involve several other DNA repair pathways.

It is remarkable that the behavior of the human Smc5/6 complex is so similar to that of the budding yeast Smc5/6 complex described in an accompanying paper by Gutierrez-Escribano et al. (2020). Both the yeast and human complexes associate tightly with nucleic acids, recognize supercoiled DNA structures and compact DNA with high efficiency. These are unusual biochemical activities to harbour in a single DNA repair enzyme. Likewise, both of our studies have identified Smc6 ATPase/CC neck as a likely interaction hub for other subunits of the Smc5/6 complex. Collectively, these similarities indicate that the absence of Nse2 subunit in the human complex does not negatively impact the biochemical activities reported herein, consistent with the fact that Nse2 is not essential for cell viability in metazoans (Kliszczak et al., 2012; Verver et al., 2016; Zheng et al., 2017). One possible difference we observed between the yeast and human complexes lies in the configuration of the SMC arms. The arms of the yeast complex seem to adopt a predominantly folded conformation, while our EM analysis suggests an extended conformation for human SMC arms. While this may appear as a discrepancy, recent structural studies indicate that SMC complexes can adopt distinct folded configurations (Burmann et al., 2019; Lee et al., 2020). Small differences in purification, imaging conditions or nucleotide status may favor one configuration over the other, thus explaining the different folded states of the yeast and human Smc5/6 complexes in our studies. In this context, the extended and folded CC arms of Smc5/6 complexes should be viewed as alternative physiological states, not as mutually exclusive conformations. Altogether, the yeast and human studies entirely converge in their demonstrations that the Smc5/6 enzyme is a structure-specific DNA compacting machine, an exciting paradigm for SMC-mediated DNA repair reactions.

The clinical and biological implications of our findings are exemplified by the connection of the LIC syndrome to a plausible defect in the function or regulation of Smc6 ATPase head/neck region. Indeed, we have identified an interaction hub within Smc6 and shown that mutations in LIC syndrome patients map directly to the region of Nse3 that associates with the interaction hub in Smc6. The same region of Smc6 was proposed to play an important role as a potential gate for the control of DNA movement through SMC arms (reviewed in Palecek and Gruber, 2015). We infer from these observations that patients with LIC syndrome might harbor a defect in a Nse3-WH/Smc6 gate that controls transit of DNA into the Smc5/6 ring structure.

Limitations

Our DNA binding analyses indicate that the Smc5/6 complex associates tightly to nucleic acids using a standard –likely electrostatic– mode of binding. Our experiments did not address whether the Smc5/6 complex can bind DNA through topological entrapment (Kanno et al., 2015). Indeed, DNA association based exclusively on topological entrapment typically cannot be observed on linear DNA substrates (such as those used in Figure 5; Ocampo-Hafalla and Uhlmann, 2011), and additional experiments will be required to clarify this question. Future work should also focus on assessing the capacity of the Smc5/6 complex to induce DNA micro-compaction during DNA repair reactions. Our study provided a compelling demonstration of the capacity of the Smc5/6 complex to compact DNA *in vitro*, but *in vivo* visualization of this mechanism would further reinforce the paradigm we propose and provide a system to assess how ancillary effectors of the Smc5/6 complex (such as Nse2 and the elusive human homolog of yeast Nse5) might impact DNA repair reactions promoted by the core Smc5/6 complex.

STAR Methods

Resource availability

Lead contact: Requests for resources and reagents should be directed to and will be fulfilled by the Lead Contact, Damien D'Amours (damien.damours@uottawa.ca).

Materials availability: Plasmids and yeast strains generated in this study are available on request. MTA may be required to share materials, in accordance with the University of Ottawa policy on inter-institutional transfer of research materials.

Data and code availability: The datasets generated during this study are available at Mendeley [http://dx.doi.org/10.17632/35z5bfkpv3.1].

Experimental model and subject details

Yeast strains.—All yeast strains used in this study are derivative of K699/K700 (Table S2). Gene deletion strains were generated by PCR amplification as previously described (Longtine et al., 1998). Yeast growth conditions, media composition and procedures for genetic analysis were as published before (Robellet et al., 2015). For DNA-damaging experiments, yeast were dropped on solid medium containing different concentrations of MMS, 4-NQO and HU at 23 °C and 37 °C. Briefly, 5-fold dilution series of fusion yeast

strains (first spot corresponds to a culture at OD_{600} of 0.2) were spotted on solid YPD (Yeast extract, Peptone, 2% Glucose) and grown in temperature-controlled incubators for 48–72 hours before scanning the plate.

For protein overexpression in fermentor, yeast strains were grown at 32 °C in YEP with 2% lactic acid and 3% glycerol as carbon source. When OD_{600} reached 0.5–0.6, protein overexpression was induced at 23 °C by addition of galactose to a final concentration of 1.5%. For protein overexpression in incubator/shaker, yeast strains were grown at 30 °C/250 rpm in YEP with 2% raffinose as carbon source. When OD_{600} reached 0.7–0.9, protein overexpression was induced at 18 °C/250 rpm by addition of galactose to a final concentration of 2%. At the end of the experiment, yeast cells were harvested, washed with cold water and frozen by immersion in liquid nitrogen.

Method Details

Yeast fusions.—Endogenous sequences (including *SMC6* and *NSE4* promotors) were amplified by PCR from strain D4107 (wild-type, haploid). Primers were designed with overhanging sequences to facilitate DNA fragment fusion by PCR and allow addition of flexible linker-encoding sequences between genes (while preventing the addition of amino-acids due to the presence of restriction sites). The same linker sequences as those used for fusion of human genes were used in the yeast fusion constructs (see plasmids p1409 and p1410 below). All PCR products were purified by gel extraction (Qiagen) and then a mix containing Herculase II buffer, dNTPs, PFU Herculase II polymerase, and 1:1 DNA ratio *Linker-*P_{NSE4}*-NSE4* or *Linker-*P_{SMC6}*-SMC6* was incubated for two PCR cycles. Then, primers were added to extend the joined-fragments product. A similar strategy was followed to fuse P_{NSE4}*-NSE4-Linker* to *SMC5*. Final constructs were cloned into the YIplac211 integrative plasmid using XmaI and SalI restriction enzymes (New England Biolabs).

smc6Δ, *nse4Δ* and *smc5Δ* were generated in diploid strains due to the fact that subunits of the Smc5/6 complex are essential. 4μg of the *URA3*-integrative plasmids YIplac211-P_{SMC6}*-SMC6-Linker-NSE4* and YIplac211-P_{NSE4}*-NSE4-Linker-SMC5* were linearized and transformed in *SMC6/smc6Δ NSE4/nse4Δ* and *SMC5/smc5Δ NSE4/nse4Δ* strains, respectively. Positive diploid strains expressing *SMC6-Linker-NSE4* and *NSE4-Linker-SMC5* were sporulated and dissected using a Nikon 50i microscope equipped with a tetrad micro-manipulator. Finally, spores carrying the double deletion and the fusion protein were screened by PCR to confirm the genotype.

Purification of Smc5/6 dimer.—Human Smc5 and Smc6 subunits were codon-optimized for expression in yeast and subcloned in a 2μ-derived plasmid under the control of the *GAL10–1* promoter sequence, as previously done for condensin subunits (St-Pierre et al., 2009). The Smc5/6 dimer was purified from ≥14L cultures of yeast grown to an OD_{600} of 1.0 – 1.5. Yeast overexpressing human Smc5/6 dimer were lysed in a freezer mill and resuspended in buffer A (500 mM NaCl, 100 mM Tris-HCl pH 8.0 and 10% glycerol) supplemented with 20 mM imidazole, 0.5% Triton X-100, 2 mM β-mercaptoethanol (βME) and protease inhibitors (E64, PEPA, AESBF). Lysate was centrifuged at 12,000rpm for 30 minutes at 4 °C. Next, Ni-NTA resin was added to the supernatant and incubated for one

hour. Once binding was complete, resin was washed with 10CV of buffer A and then with 2CV of buffer ATP (buffer A supplemented with 2 mM ATP and 25 mM KCl). Protein was finally eluted in buffer A supplemented with 500 mM imidazole. Ni-NTA elution was then passed through a column loaded with avidin-agarose beads. Next, the avidin flow through material was loaded into a StrepTrap HP 5 mL column and washed with 10 CV of buffer A supplemented with 1 mM DTT and 0.5% Triton X-100 and then, it was followed by a wash with buffer A supplemented with 2 mM βME until UV was zero. Finally, proteins were eluted in buffer A supplemented with 2 mM βME and 20 mM desthiobiotin. Elutions containing the dimer were dialyzed in buffer A, concentrated, quantified, snap frozen and stored at −80 °C.

Purification of the Smc5/6 core complex.—Subunits of the human Smc5/6 complex were codon-optimized for expression in yeast and subcloned in 2μ-derived plasmids under the control of the *GAL10–1* promoter sequence (see Fig. 1B for a description of genes contained in overexpression plasmids and the tagging/fusion strategies). To create subunit fusions, we inserted the DNA sequence encoding GGGGGPRENLYFQGPRENLYFQGASENLYFQGGGGGGG ASENLYFQGEAG and GGGGSGGGSGGGGTRARENLYFQGASENLYFQGELENLYFQGAS linkers between the coding sequences of Nse4a and Smc5 (plasmid p1409) and Smc6 and Nse4a (plasmid p1410), respectively. The Smc5/6 core complex was typically purified from 70L cultures of yeast grown to an OD_{600} of 1.0 – 1.5. Yeast pellets overexpressing the human Smc5/6 complex (Nse4a-L-Smc5 or Smc6-L-Nse4a fusions) were lysed in a freezer mill and resuspended in buffer N (50 mM K_2HPO_4 / KH_2PO_4 pH8, 50 mM Tris-HCl pH 8.0, 500 mM NaCl, 10% glycerol, 0.5 % triton X-100, 2 mM βME) supplemented with 20 mM imidazole and protease inhibitors (E64, PEPA, AESBF). Lysate was centrifuged at 12000 rpm for 30 min at 4 °C and then Ni-NTA resin was loaded to the supernatant and incubated for one hour. Resin was washed with 10 column volumes (CV) of buffer N supplemented with 60 mM imidazole. Complex was eluted with buffer SB (50 mM Tris-HCl pH 8.0, 500 mM NaCl, 10% glycerol, 0.5% tween 20, 2mM βME) supplemented with 500 mM imidazole. Flow through of Ni-NTA purification was loaded with Ni-NTA resin for a second round of purification. Next, elution fractions were loaded into a StrepTrap HP 5mL column and washed with 10 CV of buffer SB supplemented with 0.5% Triton X-100. Proteins were eluted with 5 CV of buffer GB (25 mM K_2HPO_4/KH_2PO_4 pH8, 500 mM NaCl, 10% glycerol and 2 mM βME) supplemented with 20 mM desthiobiotin. Next, the elution was loaded in a GSTrap 5 mL column, washed with 10 CV of buffer GB and the Smc5/6 complex was eluted with 5 CV of buffer GEB (50 mM Tris-HCl pH 8.0, 500 mM NaCl, 10% glycerol and 2 mM βME supplemented with 10 mM of Glutathione). Linker, poly-histidine, Strep-tag II and GST tags were cleaved by an overnight digestion with 1 mg of TEV protease per 4 mg/mL of fusion protein. Digestion was carried out in GEB buffer supplemented with 1 mM DTT. Digestion product was loaded into a Superose 6 10/300 size exclusion chromatography column in GF buffer (50 mM Tris-HCl pH 8.0, 500 mM NaCl, 10% glycerol and 2 mM βME) in order to remove the cleaved tags, digested linker and TEV. Elution fractions containing highly purified and stoichiometric complex were concentrated, quantified, snap frozen and stored at −80 °C. Although purification experiments shown herein were conducted with Smc5/6 complexes derived from the Nse4a-linker-Smc5 fusion

variant, we noticed that complexes derived from the Smc6-linker-Nse4a fusion could also be efficiently purified using the same procedure.

Density gradients.—Human Smc5/6 complex (80 pmoles) was applied on a continuous 5–20% sucrose density gradient (50 mM Tris-HCl pH 8, 500 mM NaCl, 0.05 mM EDTA, 6.25 mM $MgCl_2$, 0.5 mM βME). The gradient was generated in a BioComp gradient station. Ultracentrifugation was performed at 4 °C during 22 hours at 32,000 rpm in a Sorvall WX100 centrifuge (SW 41 Ti rotor, Beckman Coulter). 450 μL fractions were collected manually by pipetting from the top of the tube to the bottom and visualized by silver staining using SilverQuest Kit (Invitrogen).

A modified GraFix protocol was followed when complex stabilization was required for structural analysis (Kastner et al., 2008; Stark, 2010). Briefly, the heavy fraction (20% sucrose) of a 5–20% sucrose gradient (50 mM HEPES pH8, 500 mM NaCl, 0.05 mM EDTA, 6.25 mM $MgCl_2$, 0.5 mM βME) was supplemented with 0.15% glutaraldehyde. The gradient was generated in a BioComp gradient station. The samples were ultracentrifuged and fractionated as above and immediately quenched by addition of 450 μL of buffer Q (100 mM Tris-HCl pH 8, 500 mM glycine, 300 mM NaCl and 2% glycerol). Samples were visualized by silver staining.

Negative stain electron microscopy and image analysis.—Carbon-coated copper grids (Electron Microscopy Sciences, USA) were negatively glow-discharged (Agar Scientific, USA) before adsorbing 5 μl of sample, then staining with 5 μl of freshly prepared 1.5% uranyl formate (Electron Microscopy Sciences, USA). Samples were imaged at room temperature using a FEI Tecnai T12 (Eindhoven, The Netherlands) Transmission Electron Microscope equipped with a LaB6 filament and operated at 120 kV. Images were collected at defocus between 0.5–2 μm on a FEI Eagle 4k x 4k CCD camera at magnifications of ~67,000 x (pixel size 1.64 Å) or ~110,000 x (pixel size 0.99 Å). Particles were selected manually using EMAN2 (Tang et al., 2007) and extracted in 518 Å x 518 Å boxes with RELION 3.0 (Scheres, 2012). 2D averages were generated using 44 Smc5/6 complex pre-GraFix particles, 68 Smc5/6 complex post-GraFix particles, and 167 Smc5/6 dimer post-GraFix particles. Contrast transfer function correction was not implemented during image processing. For 3D image analysis, 945 post-GraFix Smc5/6 complex particles were imaged at ~42,000x (pixel size 2.59 Å) and aligned using the CL2D algorithm (Sorzano et al., 2010) from Xmipp (Sorzano et al., 2004). An initial 3D model was generated from 2D classes using RANSAC (Vargas et al., 2014) and the volume was refined with single particles in RELION 3.0 (Scheres, 2012) after low-pass filtering to 60 Å. Default refinement parameters were used without masking nor imposing symmetry. The final 3D EM map was visualized using UCSF Chimera (Pettersen et al., 2004).

DNA binding and ATPase assays.—The DNA binding activity of human Smc5/6 complex was determined by electrophoretic mobility shift assay (EMSA) according to a modified protocol previously used in our laboratory (Roy and D'Amours, 2011; Roy et al., 2011). DNA substrates were φX174 (ssDNA substrate; 5386 bp) and EcoRI-digested pBluescript II KS (dsDNA substrate; 2961 bp). Briefly, protein-DNA binding assays were carried out in 25 μL of reaction buffer (10 mM Hepes pH 7.5, 160 mM NaCl, 7 mM $MgCl_2$,

20% glycerol and 2 mM βME) containing 50 ng of DNA substrate (either ss or dsDNA) and various molar excess amounts of Smc5/6 dimer or core complex. After incubation at 30 °C for 30 min, the reactions were terminated by addition of an equal volume of 1.6% low melting point agarose containing 1 μL of loading buffer (0.6% glycerol, 0.005% bromophenol blue, 0.005% xylene cyanol). The mixture was then loaded on a 0.8% TAE-agarose gel and the DNA was resolved by electrophoresis for 16 hours at 4 °C. DNA was stained in agarose gels with SYBR Gold (ssDNA) or SYBR Green I (dsDNA) reagents and the resulting fluorescent signal was imaged using a Thyphoon FLA 9500 scanner. Free DNA was quantified using ImageJ software. For each condition, unbound DNA was quantified and plotted as a percentage of the total DNA loaded in the no-protein lane. Curve fitting of affinity constants and Hill coefficients were determined using GraphPad Prism 7 (GraphPad Software Inc). ATPase assays were performed as previously described with minor modifications (Roy et al., 2011). In this assay, the Smc5/6 ATPase showed a nucleotide hydrolysis rate of 0.049 ± 0.009 mol/sec/mol of protein, similar in range to the activity reported for condensin (Kimura and Hirano, 2000), and vastly superior to the activity of the individual Smc5 monomer (0.0019 ± 0.0005 mol of ATP per mol of Smc5 per second, as measured by (Roy et al., 2011)).

Magnetic tweezers experiments.—Linear DNA fragments used in single-molecule supercoiling relaxation experiments were derived from the plasmid pNG1175 (9702 bp), a slightly modified version of pFOS-1 (9691 bp, New England Biolabs) (Keenholtz et al., 2017). pNG1175 was linearized by cutting at nearby SpeI and ApaI restriction sites; the resulting linear molecule was ligated to ≈900 bp PCR products carrying either biotinylated or digoxigenin-labeled nucleotides, prepared with SpeI and ApaI-compatible ends, respectively. The resulting linear constructs were 11.4 kb in length, with roughly 900-bp of biotin- and digoxigenin-labeled DNA at their ends, allowing multiple tethering of the ends to streptavidin- or anti-digoxigenin-coated surfaces. The multiple tethers constrain the two DNA strands sufficiently that they may be supercoiled by rotation of the magnetic particle.

Flow cells were assembled for each experiment and contained 2.8 μm streptavidin coated paramagnetic beads (Invitrogen Dynabeads, M-270) tethered to the surface of an anti-digoxigenin coated glass coverslip via a linear pNG1175 DNA molecule with biotinylated and digoxigenin-labeled ends (Fig. 6A). Flow cell contents were viewed with a bright field microscope and a 100× 1.3NA oil immersion objective (Olympus). Translation in the z direction of a permanent magnet under the objective stage controlled the force on the bead while 360° rotations of the magnet controlled the linking number of the tethered DNA molecule. Bead position in three dimensions was tracked with custom lab-written software (LabView, National Instruments), which uses an untethered bead nonspecifically bound to the glass surface as a reference point. Position fluctuations in the x-y plane were used to calibrate the force on the tethered beads while changes in the z direction relative to the reference bead were used to measure the tether extension (Skoko et al., 2004). Experiments recorded DNA extension for approximately 1000 sec, at approximately 100 measurements per second.

Single-molecule experiments to study DNA compaction were carried out in an assay buffer containing 10 mM HEPES pH 7.5 and 50 mM potassium glutamate at 25 °C. An additional

1 mM nucleotide (ATP, ADP or ATPγS) along with 1 mM $MgCl_2$ was included as noted. The Smc5/6 core complex was added to a 200 μL mixture of assay buffer for a final concentration of 5 nM and immediately added to flow cells with tethers initially held at 4 pN force, with force reduced to 0.30 pN (or other forces as indicated for force-titration experiments) following addition of enzyme solution to the flow cell.

There are variations in tether length due to adhering of varied amounts of the 900 bp (300 nm) labeled ends, as well as due to random variation in the bead sizes, position on the bead of DNA tethering, and bead optical properties, which affect the precise location of the focal plane that determines the inferred position of the beads in the vertical direction. These effects lead to variation of initial length in the few hundred nanometer range as observed.

Single-molecule supercoil/plectoneme capture experiments were carried out following the same method except for the use of a buffer containing 100 mM potassium glutamate. The effect of increased potassium glutamate on single-molecule experiments could act at two levels: stimulation of an otherwise silent activity in the Smc5/6 complex and/or suppression of another activity in the complex. Potassium glutamate is known to stabilize many protein-DNA complexes (Cheng et al., 2016 and reference cited therein). Glutamate also has the ability to relieve inhibition induced by some salts in enzymatic reactions (Griep and McHenry, 1989). It is conceivable that higher concentrations of potassium glutamate in single-molecule experiments could stabilize Smc5/6 complex binding to plectonemic DNA or stimulate a dormant activity in the complex, but more work is required to define the detailed effects of buffers/salts on Smc5/6 activity.

Protein crosslinking and mass spectrometry.—Proteins were purified as described above. A total of 50 μg of protein in buffer C (50 mM HEPES pH8, 500 mM NaCl, 5% glycerol) was crosslinked at room temperature for 5 minutes with 0.3 mM DSS (Thermo Fisher) or with DMTMM (Sigma Aldrich). Note that DSS is a Lys-Lys crosslinker whereas DMTMM is a Lys-Asp or Lys-Glu crosslinker. Crosslinking reactions were then quenched by addition of 10 μL of 1 M Tris-HCl pH 8. Samples were then analyzed by mass spectrometry at the Proteomics Core Facility in IRIC (Montreal, Canada) by scientists with experience in the XL-MS procedure (Courcelles et al., 2017). To ensure our XL-MS analysis does not lead to false-positive identifications, all procedures were performed with enzyme preparations that are active in biochemical assays reported herein. Furthermore, MS spectra identified in our XL analysis were inspected manually and their identity re-confirmed by direct observation to ensure they truly represent crosslinked peptides, as previously described (Courcelles et al., 2017). Finally, XL reactions were not conducted to full saturation to avoid capture of spurious interactions and formation of unspecific XLs. Detailed circular maps of inter-subunit and intra-protein crosslinks were generated using Circos software (Krzywinski et al., 2009).

Immunoblot analysis.—Cell lysates were prepared from exponential cultures of yeast grown at 23 °C or 37 °C using the TCA glass-bead method (Foiani et al., 1994). Lysates were subsequently resolved by SDS-PAGE and processed for immunoblot analysis using an anti-HA antibody 12CA5 (1:2500 dilution; MilliporeSigma) and an anti-mouse IgG antibody (1:5,000 dilution; Cytiva), as described by St-Pierre et al. (2009). A 12CA5 cross-

reacting band was used as a loading control, as previously described (Gallego et al., 1997). Band intensity on immunoblots was measured using Image J software (NIH, USA).

Quantification and statistical analysis

Data are presented as means ± SEM. All statistical analyzes were performed using GraphPad Prism 7 (GraphPad Software Inc) and statistical significance threshold was set at *p*-value = 0.05. Where indicated in figure legends, we performed an analysis of variance (ANOVA) followed by a Dunnett's *post hoc* test.

Supplementary Material

Refer to Web version on PubMed Central for supplementary material.

Acknowledgments

We thank members of the D'Amours laboratory for their comments on the manuscript and Peter Stirling (UBC) for sharing *nse1/3/4* mutant strains. This work was supported by grants from CIHR to DD (FDN–167265) and NSERC to JMP (DG RGPIN-2015-05776). Work at NU was supported by the NIH grants R01-GM105847, U54-CA193419 (CR-PS-OC) and a subcontract to grant U54-DK107980 (4D Nucleome). DD is supported by a Canada Research Chair in Chromatin Dynamics & Genome Architecture. DS & AS were supported by postdoctoral fellowships from the FRQS (#29086 & #33382) and NSERC (#487769-2016), respectively.

References

Alt A, Dang HQ, Wells OS, Polo LM, Smith MA, McGregor GA, Welte T, Lehmann AR, Pearl LH, Murray JM, et al. (2017). Specialized interfaces of Smc5/6 control hinge stability and DNA association. Nat Commun 8, 14011. [PubMed: 28134253]

Andrews EA, Palecek J, Sergeant J, Taylor E, Lehmann AR, and Watts FZ (2005). Nse2, a component of the Smc5–6 complex, is a SUMO ligase required for the response to DNA damage. Mol Cell Biol 25, 185–196. [PubMed: 15601841]

Aragon L (2018). The Smc5/6 Complex: New and Old Functions of the Enigmatic Long-Distance Relative. Annu Rev Genet 52, 89–107. [PubMed: 30476445]

Baxter J, Oliver AW, and Schalbetter SA (2019). Are SMC Complexes Loop Extruding Factors? Linking Theory With Fact. Bioessays 41, e1800182. [PubMed: 30506702]

Behlke-Steinert S, Touat-Todeschini L, Skoufias DA, and Margolis RL (2009). SMC5 and MMS21 are required for chromosome cohesion and mitotic progression. Cell Cycle 8, 2211–2218. [PubMed: 19502785]

Bitard-Feildel T, Lamiable A, Mornon JP, and Callebaut I (2018). Order in Disorder as Observed by the "Hydrophobic Cluster Analysis" of Protein Sequences. Proteomics 18, e1800054. [PubMed: 30299594]

Burmann F, Basfeld A, Vazquez Nunez R, Diebold-Durand ML, Wilhelm L, and Gruber S (2017). Tuned SMC Arms Drive Chromosomal Loading of Prokaryotic Condensin. Mol Cell 65, 861–872 e869. [PubMed: 28238653]

Burmann F, Lee BG, Than T, Sinn L, O'Reilly FJ, Yatskevich S, Rappsilber J, Hu B, Nasmyth K, and Lowe J (2019). A folded conformation of MukBEF and cohesin. Nat Struct Mol Biol 26, 227–236. [PubMed: 30833788]

Chen YH, Choi K, Szakal B, Arenz J, Duan X, Ye H, Branzei D, and Zhao X (2009). Interplay between the Smc5/6 complex and the Mph1 helicase in recombinational repair. Proc Natl Acad Sci U S A 106, 21252–21257. [PubMed: 19995966]

Cheng X, Guinn EJ, Buechel E, Wong R, Sengupta R, Shkel IA, and Record MT Jr. (2016). Basis of Protein Stabilization by K Glutamate: Unfavorable Interactions with Carbon, Oxygen Groups. Biophys J 111, 1854–1865. [PubMed: 27806267]

Courcelles M, Coulombe-Huntington J, Cossette E, Gingras AC, Thibault P, and Tyers M (2017). CLMSVault: A Software Suite for Protein Cross-Linking Mass-Spectrometry Data Analysis and Visualization. J Proteome Res 16, 2645–2652. [PubMed: 28537071]

de la Rosa-Trevin JM, Quintana A, Del Cano L, Zaldivar A, Foche I, Gutierrez J, Gomez-Blanco J, Burguet-Castell J, Cuenca-Alba J, Abrishami V, et al. (2016). Scipion: A software framework toward integration, reproducibility and validation in 3D electron microscopy. J Struct Biol 195, 93–99. [PubMed: 27108186]

Doyle JM, Gao J, Wang J, Yang M, and Potts PR (2010). MAGE-RING protein complexes comprise a family of E3 ubiquitin ligases. Mol Cell 39, 963–974. [PubMed: 20864041]

Eeftens JM, Bisht S, Kerssemakers J, Kschonsak M, Haering CH, and Dekker C (2017). Real-time detection of condensin-driven DNA compaction reveals a multistep binding mechanism. Embo j 36, 3448–3457. [PubMed: 29118001]

Foiani M, Marini F, Gamba D, Lucchini G, and Plevani P (1994) The B subunit of the DNA polymerase alpha-primase complex in Saccharomyces cerevisiae executes an essential function at the initial stage of DNA replication. Mol Cell Biol 14, 923–933. [PubMed: 8289832]

Gallego C, Garí E, Colomina N, Herrero E, and Aldea M (1997) The Cln3 cyclin is down-regulated by translational repression and degradation during the G1 arrest caused by nitrogen deprivation in budding yeast. EMBO J 16, 7196–7206. [PubMed: 9384596]

Garcia-Muse T, and Aguilera A (2019). R Loops: From Physiological to Pathological Roles. Cell 179, 604–618. [PubMed: 31607512]

Griep MA, and McHenry CS (1989). Glutamate overcomes the salt inhibition of DNA polymerase III holoenzyme. J Biol Chem 264, 11294–11301. [PubMed: 2567734]

Gruber S, Arumugam P, Katou Y, Kuglitsch D, Helmhart W, Shirahige K, and Nasmyth K (2006). Evidence that loading of cohesin onto chromosomes involves opening of its SMC hinge. Cell 127, 523–537. [PubMed: 17081975]

Hudson JJ, Bednarova K, Kozakova L, Liao C, Guerineau M, Colnaghi R, Vidot S, Marek J, Bathula SR, Lehmann AR, et al. (2011). Interactions between the Nse3 and Nse4 components of the SMC5–6 complex identify evolutionarily conserved interactions between MAGE and EID Families. PLoS One 6, e17270. [PubMed: 21364888]

Irmisch A, Ampatzidou E, Mizuno K, O'Connell MJ, and Murray JM (2009). Smc5/6 maintains stalled replication forks in a recombination-competent conformation. Embo J 28, 144–155. [PubMed: 19158664]

Jeppsson K, Carlborg KK, Nakato R, Berta DG, Lilienthal I, Kanno T, Lindqvist A, Brink MC, Dantuma NP, Katou Y, et al. (2014). The chromosomal association of the Smc5/6 complex depends on cohesion and predicts the level of sister chromatid entanglement. PLoS Genet 10, e1004680. [PubMed: 25329383]

Kanno T, Berta DG, and Sjogren C (2015). The Smc5/6 Complex Is an ATP-Dependent Intermolecular DNA Linker. Cell Rep 12, 1471–1482. [PubMed: 26299966]

Kastner B, Fischer N, Golas MM, Sander B, Dube P, Boehringer D, Hartmuth K, Deckert J, Hauer F, Wolf E, et al. (2008). GraFix: sample preparation for single-particle electron cryomicroscopy. Nat Methods 5, 53–55. [PubMed: 18157137]

Keenholtz RA, Dhanaraman T, Palou R, Yu J, D'Amours D, and Marko JF (2017). Oligomerization and ATP stimulate condensin-mediated DNA compaction. Sci Rep 7, 14279. [PubMed: 29079757]

Kegel A, Betts-Lindroos H, Kanno T, Jeppsson K, Strom L, Katou Y, Itoh T, Shirahige K, and Sjogren C (2011). Chromosome length influences replication-induced topological stress. Nature 471, 392–396. [PubMed: 21368764]

Kimura K, and Hirano T (2000). Dual roles of the 11S regulatory subcomplex in condensin functions. Proc Natl Acad Sci U S A 97, 11972–11977. [PubMed: 11027308]

Kliszczak M, Stephan AK, Flanagan AM, and Morrison CG (2012). SUMO ligase activity of vertebrate Mms21/Nse2 is required for efficient DNA repair but not for Smc5/6 complex stability. DNA Repair (Amst) 11, 799–810. [PubMed: 22921571]

Krzywinski M, Schein J, Birol I, Connors J, Gascoyne R, Horsman D, Jones SJ, and Marra MA (2009). Circos: an information aesthetic for comparative genomics. Genome Res 19, 1639–1645. [PubMed: 19541911]

Lafuente-Barquero J, Luke-Glaser S, Graf M, Silva S, Gomez-Gonzalez B, Lockhart A, Lisby M, Aguilera A, and Luke B (2017). The Smc5/6 complex regulates the yeast Mph1 helicase at RNA-DNA hybrid-mediated DNA damage. PLoS Genet 13, e1007136. [PubMed: 29281624]

Lee BG, Merkel F, Allegretti M, Hassler M, Cawood C, Lecomte L, O'Reilly FJ, Sinn LR, Gutierrez-Escribano P, Kschonsak M, et al. (2020). Cryo-EM structures of holo condensin reveal a subunit flip-flop mechanism. Nat Struct Mol Biol 27, 743–751. [PubMed: 32661420]

Longtine MS, Fares H, and Pringle JR (1998). Role of the yeast Gin4p protein kinase in septin assembly and the relationship between septin assembly and septin function. J Cell Biol 143, 719–736. [PubMed: 9813093]

Marko JF, De Los Rios P, Barducci A, and Gruber S (2019). DNA-segment-capture model for loop extrusion by structural maintenance of chromosome (SMC) protein complexes. Nucleic Acids Res 47, 6956–6972. [PubMed: 31175837]

Newman JA, Cooper CD, Roos AK, Aitkenhead H, Oppermann UC, Cho HJ, Osman R, and Gileadi O (2016). Structures of Two Melanoma-Associated Antigens Suggest Allosteric Regulation of Effector Binding. PLoS One 11, e0148762. [PubMed: 26910052]

Ocampo-Hafalla MT, and Uhlmann F (2011). Cohesin loading and sliding. J Cell Sci 124, 685–691. [PubMed: 21321326]

Palecek JJ, and Gruber S (2015). Kite Proteins: a Superfamily of SMC/Kleisin Partners Conserved Across Bacteria, Archaea, and Eukaryotes. Structure 23, 2183–2190. [PubMed: 26585514]

Pebernard S, Wohlschlegel J, McDonald WH, Yates JR 3rd, and Boddy MN (2006). The Nse5-Nse6 dimer mediates DNA repair roles of the Smc5-Smc6 complex. Mol Cell Biol 26, 1617–1630. [PubMed: 16478984]

Pettersen EF, Goddard TD, Huang CC, Couch GS, Greenblatt DM, Meng EC, and Ferrin TE (2004). UCSF Chimera--a visualization system for exploratory research and analysis. J Comput Chem 25, 1605–1612. [PubMed: 15264254]

Potts PR, Porteus MH, and Yu H (2006). Human SMC5/6 complex promotes sister chromatid homologous recombination by recruiting the SMC1/3 cohesin complex to double-strand breaks. EMBO J 25, 3377–3388. [PubMed: 16810316]

Robellet X, Thattikota Y, Wang F, Wee TL, Pascariu M, Shankar S, Bonneil E, Brown CM, and D'Amours D (2015). A high-sensitivity phospho-switch triggered by Cdk1 governs chromosome morphogenesis during cell division. Genes Dev 29, 426–439. [PubMed: 25691469]

Roy MA, and D'Amours D (2011). DNA-binding properties of Smc6, a core component of the Smc5–6 DNA repair complex. Biochem Biophys Res Commun 416, 80–85. [PubMed: 22086171]

Roy MA, Dhanaraman T, and D'Amours D (2015). The Smc5-Smc6 heterodimer associates with DNA through several independent binding domains. Sci Rep 5, 9797. [PubMed: 25984708]

Roy MA, Siddiqui N, and D'Amours D (2011). Dynamic and selective DNA-binding activity of Smc5, a core component of the Smc5-Smc6 complex. Cell Cycle 10, 690–700. [PubMed: 21293191]

Scheres SH (2012). RELION: implementation of a Bayesian approach to cryo-EM structure determination. J Struct Biol 180, 519–530. [PubMed: 23000701]

Skoko D, Wong B, Johnson RC, and Marko JF (2004). Micromechanical analysis of the binding of DNA-bending proteins HMGB1, NHP6A, and HU reveals their ability to form highly stable DNA-protein complexes. Biochemistry 43, 13867–13874. [PubMed: 15504049]

Skoko D, Yoo D, Bai H, Schnurr B, Yan J, McLeod SM, Marko JF, and Johnson RC (2006). Mechanism of chromosome compaction and looping by the Escherichia coli nucleoid protein Fis. J Mol Biol 364, 777–798. [PubMed: 17045294]

Sorzano CO, Bilbao-Castro JR, Shkolnisky Y, Alcorlo M, Melero R, Caffarena-Fernandez G, Li M, Xu G, Marabini R, and Carazo JM (2010). A clustering approach to multireference alignment of single-particle projections in electron microscopy. J Struct Biol 171, 197–206. [PubMed: 20362059]

Sorzano CO, Marabini R, Velazquez-Muriel J, Bilbao-Castro JR, Scheres SH, Carazo JM, and Pascual-Montano A (2004). XMIPP: a new generation of an open-source image processing package for electron microscopy. J Struct Biol 148, 194–204. [PubMed: 15477099]

St-Pierre J, Douziech M, Bazile F, Pascariu M, Bonneil E, Sauve V, Ratsima H, and D'Amours D (2009). Polo kinase regulates mitotic chromosome condensation by hyperactivation of condensin DNA supercoiling activity. Mol Cell 34, 416–426. [PubMed: 19481522]

Stark H (2010). GraFix: stabilization of fragile macromolecular complexes for single particle cryo-EM. Methods Enzymol 481, 109–126. [PubMed: 20887855]

Strick TR, Allemand JF, Bensimon D, Bensimon A, and Croquette V (1996). The elasticity of a single supercoiled DNA molecule. Science 271, 1835–1837. [PubMed: 8596951]

Strick TR, Kawaguchi T, and Hirano T (2004). Real-time detection of single-molecule DNA compaction by condensin I. Curr Biol 14, 874–880. [PubMed: 15186743]

Styles EB, Founk KJ, Zamparo LA, Sing TL, Altintas D, Ribeyre C, Ribaud V, Rougemont J, Mayhew D, Costanzo M, et al. (2016). Exploring Quantitative Yeast Phenomics with Single-Cell Analysis of DNA Damage Foci. Cell Syst 3, 264–277 e210. [PubMed: 27617677]

Sun M, Nishino T, and Marko JF (2013). The SMC1-SMC3 cohesin heterodimer structures DNA through supercoiling-dependent loop formation. Nucleic Acids Res 41, 6149–6160. [PubMed: 23620281]

Tang G, Peng L, Baldwin PR, Mann DS, Jiang W, Rees I, and Ludtke SJ (2007). EMAN2: an extensible image processing suite for electron microscopy. J Struct Biol 157, 38–46. [PubMed: 16859925]

Torres-Rosell J, Machin F, Farmer S, Jarmuz A, Eydmann T, Dalgaard JZ, and Aragon L (2005). SMC5 and SMC6 genes are required for the segregation of repetitive chromosome regions. Nat Cell Biol 7, 412–419. [PubMed: 15793567]

van der Crabben SN, Hennus MP, McGregor GA, Ritter DI, Nagamani SC, Wells OS, Harakalova M, Chinn IK, Alt A, Vondrova L, et al. (2016). Destabilized SMC5/6 complex leads to chromosome breakage syndrome with severe lung disease. J Clin Invest 126, 2881–2892. [PubMed: 27427983]

Vargas J, Alvarez-Cabrera AL, Marabini R, Carazo JM, and Sorzano CO (2014). Efficient initial volume determination from electron microscopy images of single particles. Bioinformatics 30, 2891–2898. [PubMed: 24974203]

Verver DE, Zheng Y, Speijer D, Hoebe R, Dekker HL, Repping S, Stap J, and Hamer G (2016). Non-SMC Element 2 (NSMCE2) of the SMC5/6 Complex Helps to Resolve Topological Stress. Int J Mol Sci 17, 1782.

Yatskevich S, Rhodes J, and Nasmyth K (2019). Organization of Chromosomal DNA by SMC Complexes. Annu Rev Genet 53, 445–482. [PubMed: 31577909]

Zabrady K, Adamus M, Vondrova L, Liao C, Skoupilova H, Novakova M, Jurcisinova L, Alt A, Oliver AW, Lehmann AR, et al. (2016). Chromatin association of the SMC5/6 complex is dependent on binding of its NSE3 subunit to DNA. Nucleic Acids Res 44, 1064–1079. [PubMed: 26446992]

Zheng Y, Jongejan A, Mulder CL, Mastenbroek S, Repping S, Wang Y, Li J, and Hamer G (2017). Trivial role for NSMCE2 during in vitro proliferation and differentiation of male germline stem cells. Reproduction 154, 181–195. [PubMed: 28576919]

Highlights

- The Smc5/6 complex is an enigmatic regulator of chromosome structure and integrity
- Non-B form DNA and supercoiled substrates are efficiently recognized by human Smc5/6
- The purified Smc5/6 enzyme compacts DNA substrates in an ATP-dependent manner
- Disruption of a subunit interaction hub in Smc6 inactivates the Smc5/6 complex

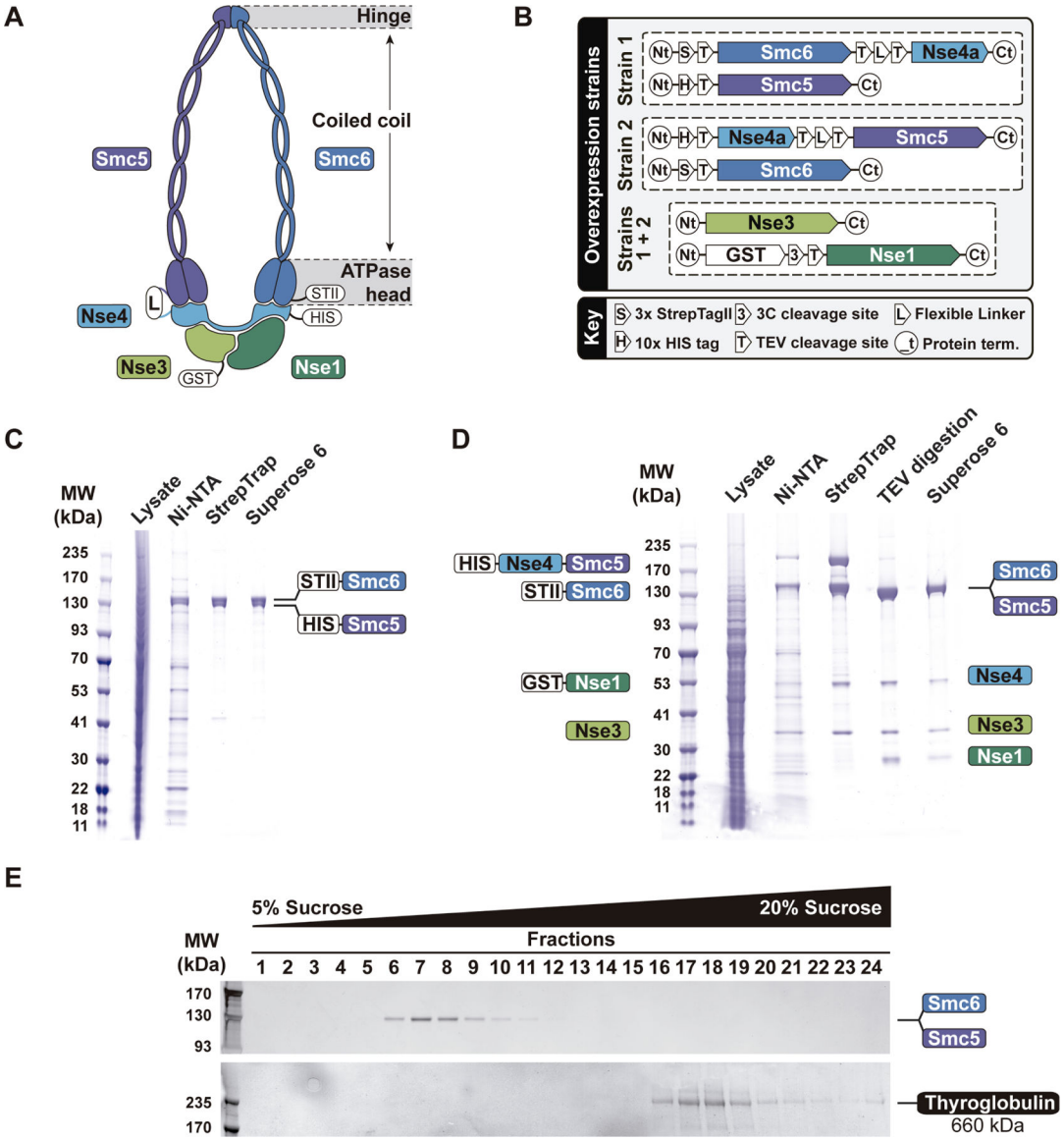

Figure 1. Purification of the Smc5/6 complex.

(A) Schematic representation of the Smc5/6 complex. **(B)** Overview of the 2 yeast strains used for Smc5/6 complex overexpression and purification. Each strain contains 2 plasmids; one for the overexpression of the Nse4/SMC subunits and the other –common to both strains– that overexpresses Nse1 and Nse3. **(C)** Representative gel showing the different chromatography steps used to purify the Smc5/6 dimer. The positions of StreptagII-Smc6 and His-Smc5 are shown on the right. **(D)** Purification steps used to isolate the Smc5/6 core complex. The positions of individual proteins prior to TEV cleavage are shown on the left of the gel, while the positions of subunits after TEV-induced removal of purification tags/linker are shown on the right of the gel. After completion of the TEV cleavage reaction, all the subunits of the Smc5/6 complex migrate in SDS-PAGE at the positions of the native full-length proteins. Note that tag-less Nse4a migrates at the same apparent mass as GST-Nse1 (*i.e.*, prior to TEV-induced removal of the GST tag). Likewise, TEV and tag-less Nse1 are

co-migrating on the gel, but TEV is removed from the Smc5/6 complex at the final gel exclusion step. **(E)** Analysis of the oligomerization status of the Smc5/6 core complex by density gradient centrifugation. See also Figures S1–3.

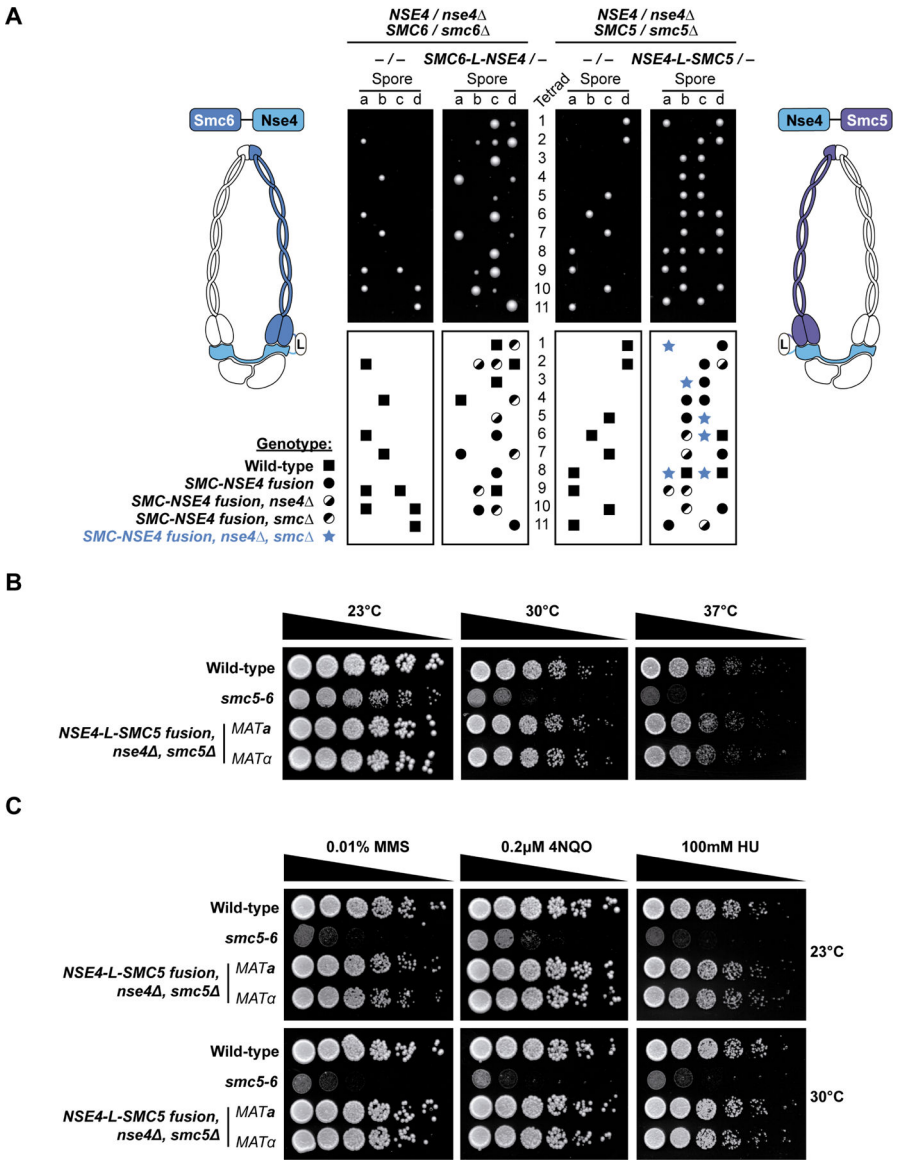

Figure 2. Functionality of Smc5/6 complexes containing Nse4-SMC fusions.

(A) Phenotype of *SMC5/6-NSE4* fusion alleles after sporulation. One copy of *NSE4* and either *SMC5* or *SMC6* were deleted in diploid yeast strains expressing Nse4-linker-Smc5 or Smc6-linker-Nse4 fusion proteins. The linker sequence and fusion strategy employed in these strains are identical to those used to purify the human subunits, except that yeast Smc5, Smc6 and Nse4 protein sequences were used to allow complementation of *nse4Δ*, *smc5Δ* and *smc6Δ* deletions. Diploid strains of the indicated genotype were sporulated and haploid spores micromanipulated on solid growth medium. The viability of spores was scored after 3 days of germination, and their genotypes are represented schematically under the growth plates. –/– and *NSE4-L-SMC*/– indicate the absence or presence of fusion alleles at the *URA3* locus of parental/diploid yeast. **(B-C)** Proliferation capacity of two independent *smc5Δ nse4Δ* clones (*MAT**a*** and *MAT**α***) expressing the Nse4-linker-Smc5 fusion protein was assessed by serial dilution assay on solid medium. After plating, cells were grown for

2–3 days at the indicated temperatures (23 °C, 30 °C and 37 °C; panel B) in the absence or presence of DNA damaging drugs (HU, MMS or 4NQO; panel C).

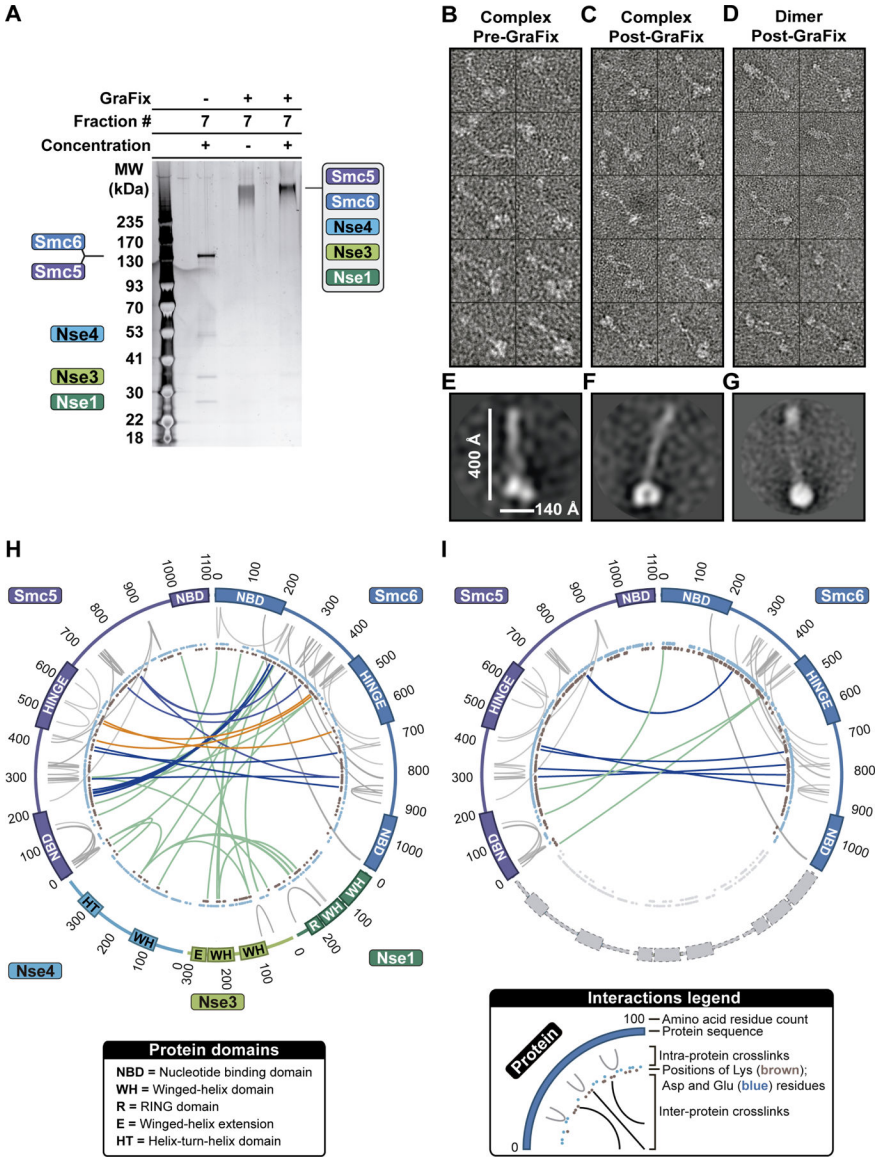

Figure 3. Shape and configuration of the Smc5/6 dimer and core complex.

(A) Stabilization of the Smc5/6 core complex using the GraFix procedure (Kastner et al., 2008). In the absence of crosslinking, subunits of the complex eluted as individual bands in sucrose density gradients, whereas they eluted as a single band of high molecular mass after GraFix crosslinking. **(B-C)** Representative single particles of Smc5/6 core complexes prior (B) and after (C) GraFix treatment. Box dimensions are 518 Å x 518 Å. **(D)** Single particle images showing the Smc5–6 heterodimer after GraFix stabilization. **(E-F)** Two-dimensional class averages of Smc5/6 core particles pre- (E) and post-GraFix treatment (F). Dimensions are represented in Å and images in E and F were reconstituted from 44 and 68 particles, respectively. **(G)** Two-dimensional class average of GraFix-stabilized Smc5/6 dimer (n = 167 particles). **(H)** Proximity maps showing intra- and inter-subunit connections within the Smc5/6 core complex. XLs identified in the MS analysis were plotted on circular diagrams corresponding to the amino-acid sequences/functional domains of Smc5/6 complex subunits.

Intra-molecular connections are shown as grey lines, whereas inter-molecular contact points are shown in the inner part of the diagram (blue lines are for XLs specific to CC domains; orange lines are for XLs connecting hinge domains; green lines are for all other XLs). **(I)** Network of inter- and intra-subunit connection points within the Smc5/6 dimer. See also Figures S3–S4 and Table S1.

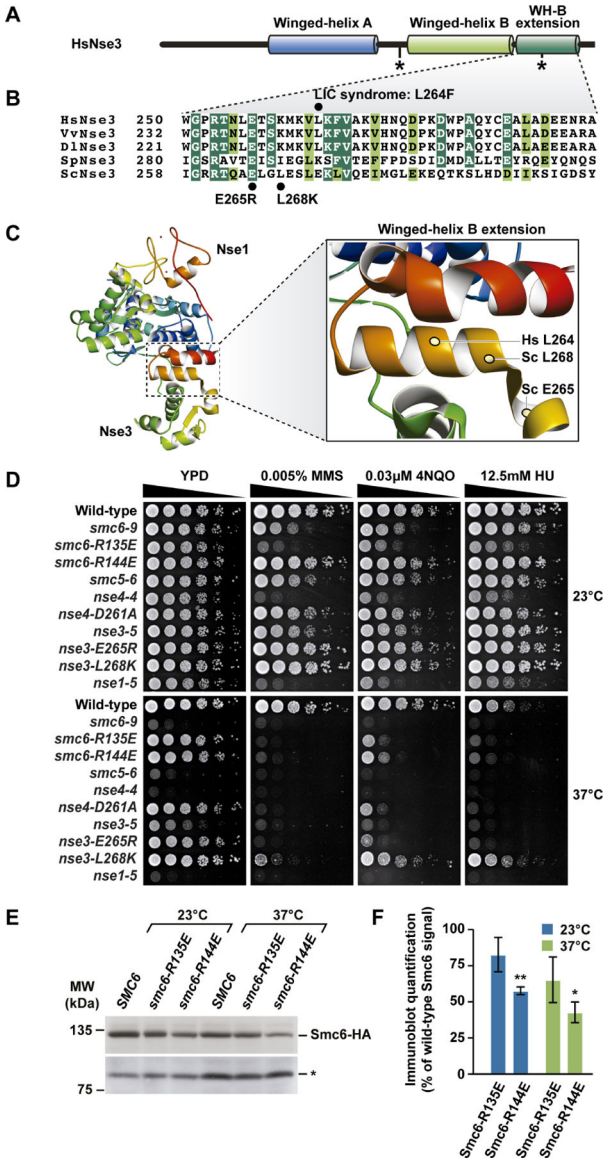

Figure 4. Impact of mutations in the WH domain of Nse3 and the ATPase/CC neck of Smc6.

(A) Schematic representation of Nse3 domain structure. The positions of LIC syndrome mutations are marked with asterisks (van der Crabben et al., 2016). **(B)** Alignment of the WH-B extension domain in eukaryotic homologs of Nse3. **(C)** Crystal structure of the Nse3-Nse1 dimer. The position of mutations created in this study is marked with yellow ovals in the magnified view (inset). The structure is PDB 3NW0 from Newman et al. (2016). **(D)** Proliferation phenotype of yeast strains carrying mutations in Smc5/6 complex components. Strains were diluted on solid medium containing DNA damaging agents and grown at the indicated temperatures for 2–4 days before recording their phenotype. **(E)** Effect of temperature on the stability of Smc6 mutants. Cell lysates of yeast grown at the indicated temperatures were resolved by SDS-PAGE and processed for immunoblot analysis. The positions of Smc6 and loading control (*) bands are shown on the right. **(F)** Quantitative analysis of Smc6 abundance determined by immunoblot. The bar graph reports the mean

protein abundance of Smc6-R135E/R144E relative to wild-type Smc6 ± SEM for 3 independent experiments. * signifies p-value ≤ 0.05 and ** a p-value ≤ 0.01 (ANOVA with Dunnett's *post hoc* test).

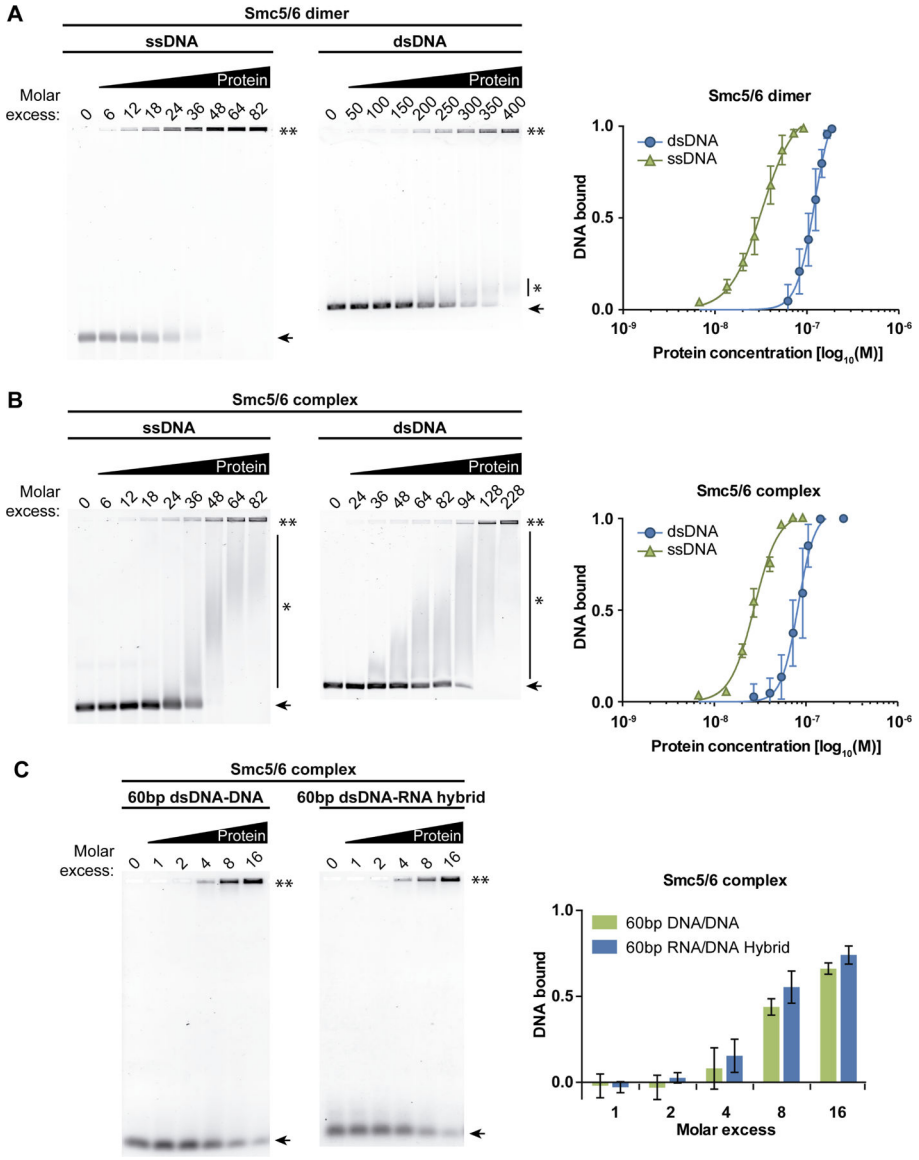

Figure 5. DNA-binding affinity and substrate preference of the Smc5/6 core complex.

The DNA-binding behavior of the Smc5–6 dimer **(A)** and core complex **(B-C)** was determined by EMSA saturation experiments using various DNA substrates. Purified complexes were incubated with the indicated nucleic acids for 30 min at 30 °C and the resulting protein-DNA complexes were resolved by electrophoresis. The molar excess of Smc5/6 complex over DNA is shown above each lane, whereas the positions of unbound and Smc5/6-bound DNA substrates are marked by arrowheads and asterisks, respectively. The graphs next to the agarose gels show the quantification of DNA-binding activity. The data reported in the graphs is the mean DNA binding ± SE of ≥3 independent experiments. See also Figure S5A.

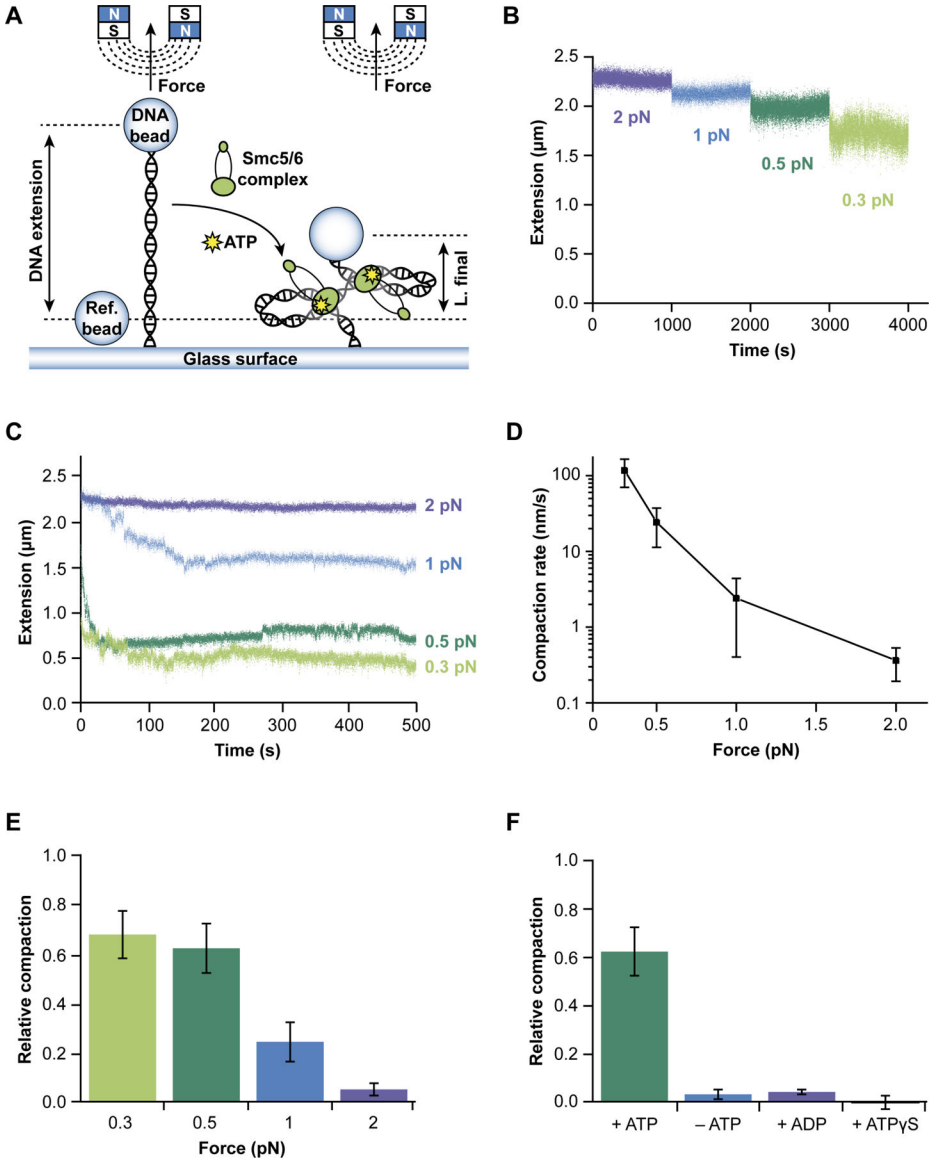

Figure 6. Compaction of DNA by the Smc5/6 complex.

(A) Schematic representation of magnetic tweezers single-DNA compaction assay. **(B)** DNA extension measured following addition of 5 nM Smc5/6 complex (added slightly before t=0) with no nucleotide. As force was reduced from 2 pN to 0.3 pN, there was no compaction observed; the reduction of length is just that expected from thermal bending fluctuations of DNA, also responsible for the increased Brownian motion around the stable average DNA extension. **(C)** DNA extension following addition of 5 nM Smc5/6 complex (at t = 0) plus 1 mM ATP (separate curves are from separate experiments). At each force, compaction occurred, with more rapid and more complete compaction at lower forces. **(D)** Compaction rate in the presence of 1 mM ATP at 0.5 pN force measured from a series of 4 experiments of the type shown in panel C for each force (note logarithmic rate scale). A rapid increase in compaction rate with decreasing force (essentially shut off above 1 pN) was observed, indicative of a DNA-loop-capture process of compaction. **(E)** Total compaction (ratio of

change in extension to initial extension) in a series of 4 experiments at different forces, indicating that compaction is more complete at lower forces, and essentially shut off above 1 pN. **(F)** Total compaction at 0.5 pN in the presence of various nucleotides (0 and 1 mM ATP, 1 mM ADP, and ATPγS). All error bars indicate SEM.

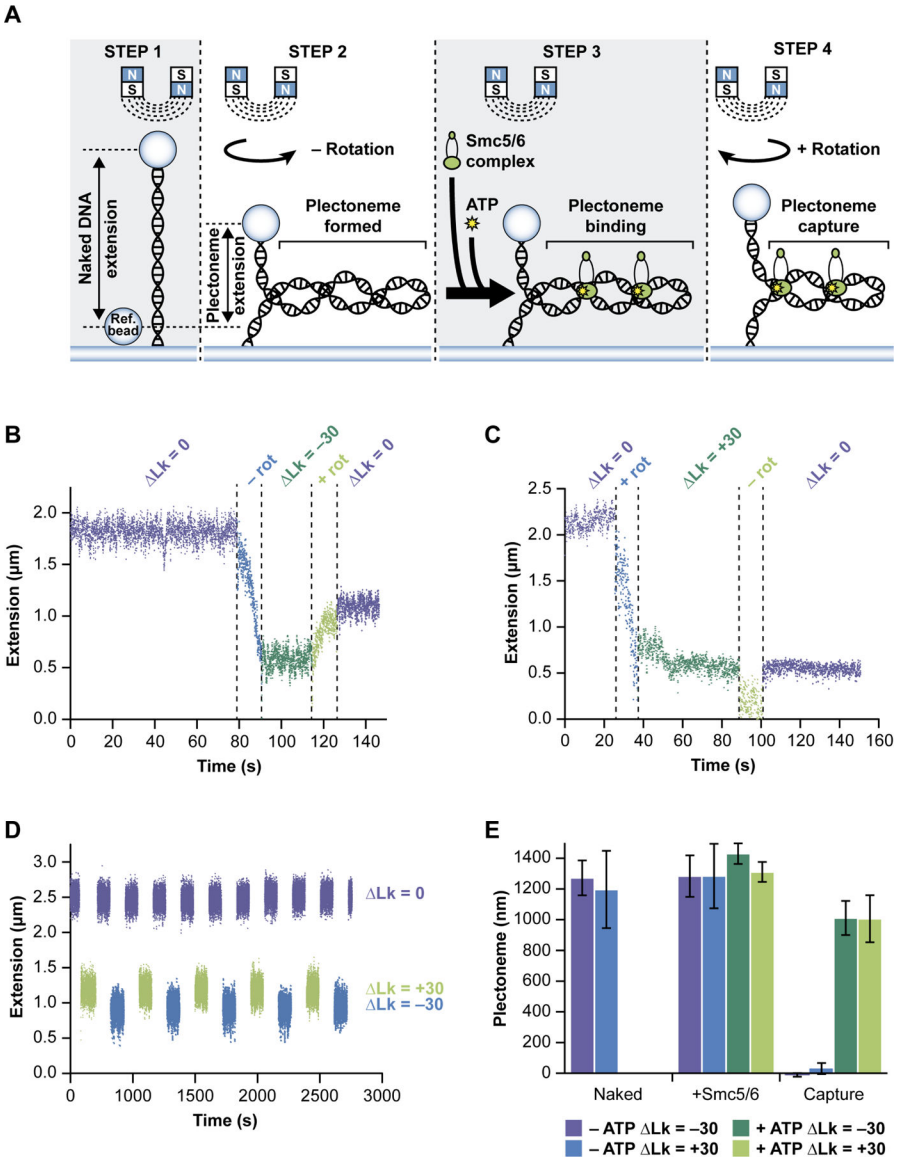

Figure 7. Capture of DNA by the Smc5/6 core complex requires supercoiling and ATP.

(A) Schematic representation of the reaction steps in the plectoneme/supercoil capture experiment conducted under increased salt conditions. **(B)** At 100 mM potassium glutamate and 1 mM ATP, a 10 kb DNA under 0.3 pN force has stable extension (purple points, left); following increase of linking number to ΔLk = −30 (blue), the molecule forms plectonemic supercoils (dark green points); when linking number is returned to ΔLk = 0, only part of the DNA length contained within the plectoneme is returned (purple points, right); about 1000 nm of length has been “captured” by the Smc5/6 core complex. **(C)** Experiment similar to B showing capture of supercoiled DNA by the Smc5/6 core complex following supercoiling to ΔLk = +30 and return to ΔLk = 0. **(D)** In the absence of ATP, linking number can be reversibly and repeatedly cycled between ΔLk = 0, +30 and −30 with no capture of supercoiling by the Smc5/6 complex. **(E)** Averages of capture experiments over a series of 5 trials show that a large fraction of the DNA length change resulting from plectonemic

supercoiling can be captured by the Smc5/6 core complex in the presence of ATP (*i.e.*, right bars; equivalent to step 4 in panel A). Changes observed in DNA extension/length are expressed as plectoneme size (nm) in the graph. The initial size of plectonemes formed with naked DNA (left bars; equivalent to step 2 in panel A) or in the presence of 5 nM Smc5/6 core complex (central bars; step 3) are shown for comparison. Each bar shows mean and SEM. See also Figure S5B,C.

KEY RESOURCES TABLE

REAGENT or RESOURCE	SOURCE	IDENTIFIER
Antibodies		
Mouse monoclonal anti-HA antibody (12CA5)	MilliporeSigma	Cat#11583816001
Anti-mouse IgG, Sheep polyclonal antibody (HRP-conjugated)	Cytiva	Cat#NA931
Bacterial and Virus Strains		
XL10-Gold ultracompetent cells	Agilent	Cat#200315
Biological Samples		
Chemicals, Peptides, and Recombinant Proteins		
AcTEV™ protease	Thermo Fisher Scientific	Cat#12575015
SYBR Gold	Invitrogen	Cat#S11494
SYBR Green I	Invitrogen	Cat#S7563
Critical Commercial Assays		
QuikChange Lightning multi site-directed mutagenesis kit	Agilent	Cat#210513
Immobilon Crescendo Western HRP substrate	MilliporeSigma	Cat# WBLUR0500
Deposited Data		
Raw and analyzed data	This paper	http://dx.doi.org/10.17632/35z5bfkpv3.1
Experimental Models: Cell Lines		
Experimental Models: Organisms/Strains		
Saccharomyces cerevisiae strain background K699/K700 (see Table S2 for a complete list of strains used in this study)	This paper	N/A
Oligonucleotides		
Recombinant DNA		
YIplac211 plasmid	ATCC	Cat#87593
Plasmid 1409: AgeI-Nterm_hSmc5-LINKER-AvrII	This paper	N/A
Plasmid 1410: SacI-LINKER-Nterm_hNSE4a-BamHI	This paper	N/A
2u plasmid for protein overexpression in budding yeast	St-Pierre et al., 2009	N/A
pNG1175	Keenholtz et al., 2017	N/A
φX174 ssDNA	New England Biolabs	Cat#N3023L
pBluescript II KS dsDNA	Agilent	Cat#212207
Software and Algorithms		
EMAN2	Tang et al., 2007	https://blake.bcm.edu/emanwiki/EMAN2
RELION 3.0	Scheres, 2012	https://github.com/3dem/relion
Xmipp	Sorzano et al., 2004	https://github.com/I2PC/xmipp
UCSF Chimera	Pettersen et al., 2004	https://www.cgl.ucsf.edu/chimera/
ImageJ	Schneider et al., 2012	https://imagej.nih.gov/ij/
Prism 7	Graphpad	www.graphpad.com
LabVIEW	National Instruments Corp	https://www.ni.com/en-ca/shop/labview.html
Circos	Krzywinski et al., 2009	www.circos.ca
Other		